DESIGN OF A MILLIMETER WAVE WAVEGUIDE BANDPASS FILTER

FOR FUTURE 5G MOBILE NETWORKS

By

LIM YUAN PING

18285

Dissertation submitted in partial fulfilment of

the requirements for the

Bachelor of Engineering (Hons)

(Electrical & Electronic)

JANUARY 2017

Universiti Teknologi PETRONAS

Bandar Seri Iskandar

31750 Tronoh

Perak Darul Ridzuan

CERTIFICATION OF APPROVAL

DESIGN OF A MILLIMETER WAVE WAVEGUIDE BANDPASS FILTER

FOR FUTURE 5G MOBILE NETWORKS

by

Lim Yuan Ping

18285

A project dissertation submitted to the

Electrical & Electronic Engineering Programme

Universiti Tekmologi PETRONAS

in partial fulfilment of the requirement for the

BACHELOR OF ENGINEERING (Hons)

(ELECTRICAL & ELECTRONIC)

Approved by,

_____ _____

Assoc. Prof. Dr. Wong Peng Wen   Dr. Cheab Sovuthy

UNIVERSITI TEKNOLOGI PETRONAS

TRONOH, PERAK

January 2017

CERTIFICATION OF ORIGINALITY

This is to certify that I am responsible for the work submitted in this project, that the original work is my own except as specified in the references and acknowledgements, and that the original work contained herein have been undertaken or done by unspecified sources and persons.

_____

Lim Yuan Ping

ABSTRACT

In this dissertation, the design of a WR-34 band (22-33 GHz) iris waveguide bandpass filter with 28 GHz center frequency and with a relative bandwidth of 2.03% is presented. An insertion loss method with a Chebyshev polynomial is used to synthesize the desired filter response. To validate the filter design, a simulation model is developed using the *ANSYS High Frequency Structure Simulator* (HFSS) software. The S-parameters simulation results indicate that the center frequency of the filter is 27.995 GHz. The lower stopband frequency (fp1) is 27.71 GHz while the upper stopband frequency (fp2) is 28.28 GHz. Therefore, the passband ranges from 27.71 GHz to 28.28 GHz, with a relative bandwidth of 2.03%. The return loss for the entire passband is better than 7.8dB. The corresponding upper and lower stopband insertion loss measurements of the filter are better than 40dB at 27.25 GHz and 28.75GHz, respectively. The filter also achieves a 570 MHz bandwidth with S11 ≤ -7.8 dB and S21 ≤ 1dB. In summary, the simulation results ascertain that the designed iris waveguide bandpass filter can serve as a viable filtering device to exploit the millimeter-wave band, in order to offer a large bandwidth and a fast data transfer rate for satisfying the growing demand of spectrum based services in future 5G mobile networks.

ACKNOWLEDGEMENTS

First and foremost, I would like to express my gratitude to my Final Year Project (FYP) supervisor, Assoc. Prof. Dr. Wong Peng Wen for his invaluable guidance and enthusiastic support throughout the whole journey of my project. His wide knowledge in the domains of microwave, waveguide filter design, and telecommunication network has been a great help for me toward the completion of my FYP within the timeline. He has inspired me a lot to think of many interesting areas of research in telecommunication. In addition, his caring, understanding and trusting attributes have provided me a good assurance for carrying out this dissertation project.

My sincere thanks are due to my project co-supervisor, Dr. Cheab Sovuthy, for his unselfishly teaching and sharing knowledge of software programs and valuable help throughout the whole FYP duration. He has assisted me immensely in understanding the filter design technique, derivation of the waveguide filter mathematical model, as well as the simulation work. I have learned a lot from him.

Special thanks are due to the microwave team that includes post graduate students from Universiti Teknologi PETRONAS for their help, innovative ideas and suggestions. I appreciate their uttermost effort in guiding me toward the completion of this project. Thousand thanks are due to those who have either directly or indirectly helped me throughout the whole journey of my dissertation. I am thankful for all their assistance and encouragement.

Lastly, I wish to acknowledge that this dissertation would not have been accomplished without the love, encouragement, understanding, patience and devotion of my family members. Without their support, I would not be able to complete this project.

TABLE OF CONTENTS

LIST OF FIGURES

LIST OF TABLES

ABBREVIATIONS AND NOMENCLATURES

HFSS	**High Frequency Structure Simulator**
FYP	**Final Year Project**
CAGR	**Compound Annual Growth Rate**
UHF	**Ultra-High Frequency**
SHF	**Super High Frequency**
EHF	**Extremely High Frequency**
IoT	**Internet of Thing**
WR	**Rectangular Waveguide (US)**
TE	**Transverse Electric**
TM	**Transverse Magnetic**
TEM	**Transverse Electromagnetic**
GPS	**Global Positioning System**
AM	**Amplitude Modulation**
FM	**Frequency Modulation**
MATLAB	**Matrix Laboratory**

CHAPTER 1

INTRODUCTION

1.1 Background of Study

Mobile communication is one of the most important and successful technologies in our daily life. It has become an indispensable part of over 5 million people around the world owing to the technology breakthroughs and attractive value propositions [1, 2]. The drastic rise of smart device users, increase in video streaming and growth in data applications such as online banking, online shopping, gaming and navigation have resulted in an unprecedented growth of mobile data traffic. As a result, customers are always obsessed with a variety of spectrum based services. Mobile data traffic is predicted to grow in the foreseeable future at an 108% compound annual growth rate (CAGR) [2, 3] over the next ten years. Customers are expected to experience a slower service, and network congestion is expected to occur due to imbalance supply and demand. In order to support the tremendous demands on mobile data traffic, researchers are motivated to overcome the global bandwidth shortage by exploring the millimeter-wave frequency spectrum for the next generation 5G mobile networks[1, 2, 4-11].

Today, we are using the Ultra High Frequency (UHF) band ranging from 300 MHz to 3 GHz in almost all commercial communication channels including TV, satellite communication, cellular, GPS, Zigbee/Bluetooh and AM/FM radio [1, 2]. On the other hand, there is still a large spectrum in the 3-300 GHz range remains under-utilized. The spectrum in the range between 3-30 GHz is generally classified as the Super High Frequency (SHF) band, while 30-300 GHz is classified as the Extremely High Frequency (EHF) band. Since both SHF and EHF bands share similar propagation characteristics and their wavelengths are in the range from 1 to 100mm, the 3-300 GHz spectrum is normally denoted as the millimeter-wave (mm-wave) band.

Millimeter-wave communication is a promising technology that can be exploited as the wireless backbone for the next generation of 5G mobile networks. A millimeter-wave communication system has a large bandwidth, which can be translated to provide a fast data transfer rate up to multi-gigabits-per-second [1, 2, 4-11] from a distance of up to few kilometers to meet the growing demand of spectrum usage. Indeed, 5G millimeter-wave communication has a clear vision, that is to accommodate the environment of Internet of Things (IoT) and provide Big-Data based platforms to billions of users deploying connected smart devices autonomously in seamless manner.

1.2 Problem Statement

Nowadays, with an increased demand of spectrum-based services that leads to a global shortage, revolutionary 5G networks with unprecedented data speeds are inevitable. In this context, a filter is a vital component to segregate between the desired and undesired signal frequencies for future 5G mobile networks.

The key problem in filter designs is that the passband loss is inversely proportional to the filter bandwidth. Therefore, an extremely high resonator Q factor must be used for the purpose of very narrow band applications, in order to realize the design of a very sharp filter with a low passband loss.

The planner Microstrip filter cannot be used to design a filter at the millimeter-wave band due to its inherent small Q factor, large insertion loss, and poor stopband suppression [12-15]. Similarly, the coaxial filter is not a suitable candidate because it gives a Q factor of at most 5,000, and the cut-off frequency is limited.

The aforementioned problems in the current filter technologies lead to the need for innovation in waveguide filters. The waveguide filter offers a very high Q resonator factor, achieves low passband loss, insertion loss, and high suppression requirements [12-15]. Indeed, the waveguide filter can be realized as a viable technology to be used in 5G cellular communication networks. In principle, the electromagnetic wave energy is propagated through the air inside the guide, rather than other conventional filters whereby the electromagnetic wave energy propagates in a conductor. The designed bandpass filter will exploit this advantage for improving the performance in terms of an increased bandwidth, leading to a higher data transfer rate to meet the demand of fast spectrum-based services.

1.3 Objectives of Study

The objectives of this project are two-fold:

- To design a millimeter-wave iris waveguide bandpass filter to discriminate between the desired and undesired frequencies signals for future 5G communication networks;
- To simulate the millimeter-wave waveguide bandpass filter by using the HFSS simulation software as well as analyze and compare the results with those from theoretical models.

1.4 Scope of Study

With respect to the objectives set forth, this dissertation concentrates on the following topics as the scope of study:

- Understanding 5G technology and millimeter-wave bands;
- Understanding Maxwell equations and the basic theorem of waveguides;
- Understanding waveguide bandpass filter design techniques;
- Specifying waveguide bandpass filter specifications;
- Designing and deriving a mathematical model for the 28 GHz millimeter-wave iris waveguide bandpass filter based on the following design specifications

Passband	27.70 GHz – 28.30 GHz
Return loss	≥ 10dB
Stopband insertion loss	≥ 40dB at 27.25 GHz
	≥ 40dB at 28.75 GHz

- Learning the HFSS 3D simulation software;
- Designing the simulation model in HFSS;
- Performing S-parameters simulation using HFSS;
- Tuning and Optimizing the waveguide filter parameters;
- Analyzing the waveguide filter performance.

1.5 Dissertation Organization

The dissertation is composed of 5 chapters, including this introduction chapter. The introduction chapter presents the background of the project, the problem statement, the objectives and scope of study. Chapter 2 mainly concentrates on the literature review. It contains all relevant theories, hypotheses, and data which are relevant to the objectives and scope of this project.

Chapter 3 discusses the methodology to achieve the objectives of the project. The project methodology covers background research, filter specifications, mathematical model, HFSS 3D model, simulation study, filter parameter tuning and optimization.

Chapter 4 contains the simulation results and discussion. This chapter presents the findings and outcomes of the project work. Mathematical modelling and S-parameters simulation results are analyzed and discussed.

In chapter 5, conclusions of this dissertation are summarized, and suggestions for future research are provided.

CHAPTER 2

LITERATURE REVIEW

2.1 Introduction to Waveguide

A waveguide consists of a hollow metallic pipe or a conductive tube with an uniform cross-section [16, 17]. It is a structure which directs the propagation of an electromagnetic wave in a particular direction within the interior of the waveguide by confining the electromagnetic wave energy. Waveguide is a promising element for the bandpass filter design because it has a high Q factor, low passband and insertion loss, and high power handling capability [12-15] when comparing with Transverse Electromagnetic (TEM) resonators and coaxial designs. Figure 2.1 shows the two common types of waveguides: (a) a rectangular waveguide; (b) a circular waveguide.

(a)   (b)
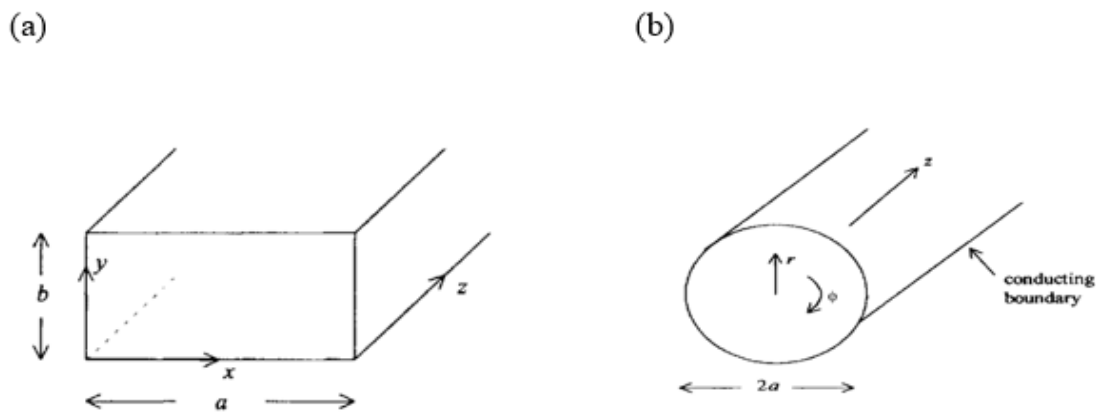
Figure 2. 1: Two common types of waveguide: (a) a rectangular waveguide; (b) a circular waveguide. [17]

2.2 Basic of TEM, TE, TM and Hybrid Propagation

According to the theory of waveguide, there are a few different types of electromagnetic waves that can propagate through the waveguide. The propagation modes vary upon the types of energy and the nature of the medium. Four basic electromagnetic waves and their corresponding propagation characteristics [17-23] are discussed in the following section, while Figure 2.2 illustrates the propagation characteristics of the TE, TM and TEM modes.

2.2.1 Transverse Electric (TE) Waves

The TE waves are sometimes known as the **H** waves**.** The main propagation characteristic of the TE waves is such that the electric field (**E**) vector is always transverse to the direction of propagation, while the magnetic field (**H**) vector is not purely transverse, i.e., $\mathbf{E_Z = 0, H_Z \neq 0.}$

2.2.2 Transverse Magnetic (TM) Waves

The TM waves are sometimes known as the **E** waves. The main propagation characteristic of the TM waves is such that the magnetic field (**H**) vector is always transverse to the direction of propagation, while the electric field (**E**) vector is not purely transverse, i.e., $\mathbf{E_Z \neq 0, H_Z = 0.}$

2.2.3 Transverse Electromagnetic (TEM) Waves

A waveguide does not support the TEM propagation mode because it is only made up of a single conductor. The main propagation characteristic of TEM waves is such that both the magnetic field (**H**) vector and electric field (**E**) are always transverse to the direction of propagation, i.e., $\mathbf{E_Z = 0}$ and $\mathbf{H_Z = 0}$

2.2.4 Hybrid Waves

The main propagation characteristic of the hybrid waves is such that both the magnetic field (**H**) vector and electric field (**E**) vector are not purely transverse to the direction of propagation, i.e., $\mathbf{E_Z \neq 0, H_Z \neq 0}$
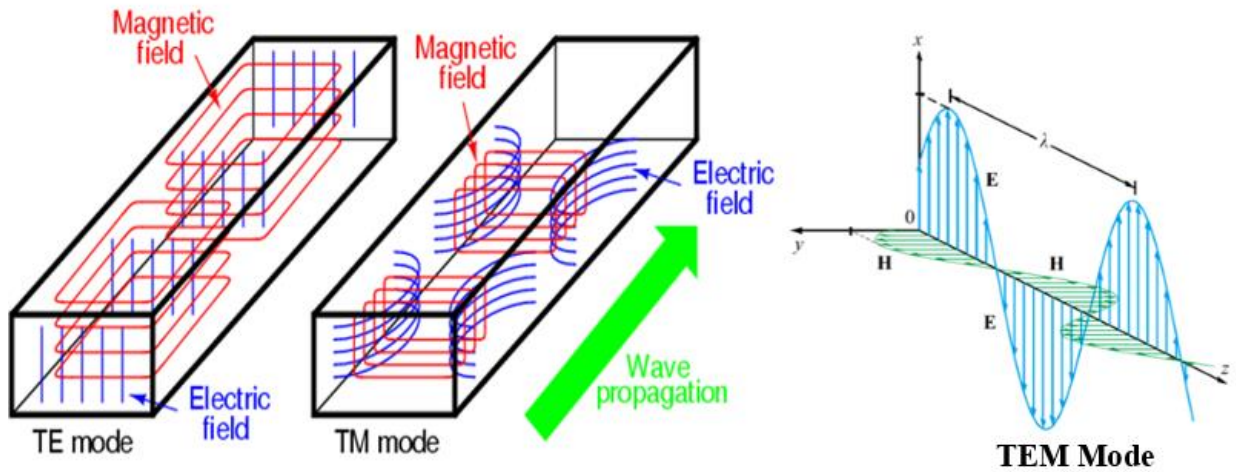
Figure 2. 2: TE, TM and TEM Propagation Mode [24].

2.3 Modes of Propagation

Electromagnetic waves travel down a waveguide in different configurations, which are known as the propagation modes. In 1995, the Institute of Radio Engineers published a set of standards to represent the rectangular waveguide propagation modes [16]. Transverse-electric waves are denoted as TEm,n, while transverse-magnetic waves are denoted by TMm,n, where both m and n are integer and the values of m and n range from 0 up to infinity[16]. In the set of standards, the number of half-wavelengths of intensity (electric and magnetic) that exist between each pair of walls are represented by m and n, where m and n are measured along the x-axis (width, a) and y-axis (height, b) of the waveguide, respectively, as shown in Figure 2.3.
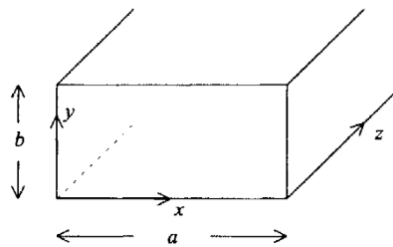
Figure 2. 3: A rectangular waveguide; where m and n are measured along the x-axis and y-axis of the waveguide, respectively[16].

Figure 2.4 shows the electromagnetic field pattern for the TE10 mode wave. TE10 mode wave is known as the dominant mode because it is the most "natural" mode. The electric field (or **E** field) vectors are parallel to each other and perpendicular to the wide face of the guide. The amplitude is the greatest at the midway between the narrow walls, and decreases to zero at the walls, in a cosine fashion. The magnetic field (or **H** field) vectors (dashed lines) are also parallel to each other and perpendicular to the electric vectors. The magnetic intensity is constant in the vertical direction across the guide section. Notice that the wave propagates in the longitude direction of the waveguide, perpendicular to the **E** and **H** vectors.
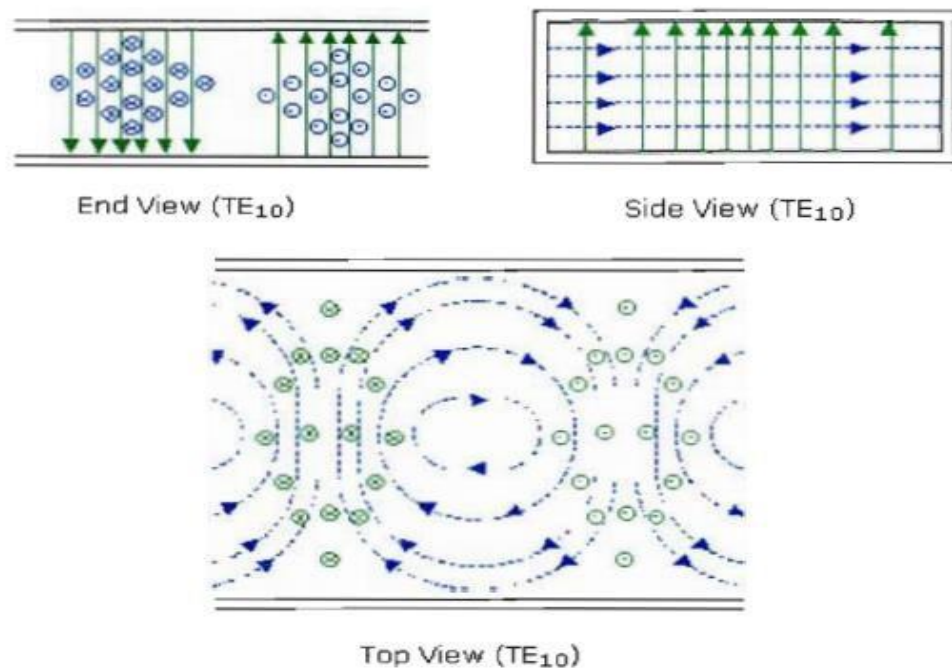
Figure 2. 4: The end view, side view and top view of the electromagnetic field pattern for TE10 mode wave[16].

A waveguide acts as a high-pass filter in that it passes only information at frequencies above the minimum or cut-off frequency. Other signals below the cut-off frequency will be attenuated. At frequencies above the cut-off frequency, when the propagation mode order becomes higher, the field configurations become more complicated. The waveguide cannot be operated at frequencies at which these higher modes can propagate. The TE10 mode is desired because it caters for the smallest possible size waveguide with respect to a given frequency of operation.

2.4 Millimeter Wave Propagation Loss

Unlike other low frequency waves, the millimeter waves open up more spectrum, but, at the same time, suffer from a higher wave propagation loss, as compared with other communication systems [1, 2, 5]. This phenomenon is related to the high carrier frequency characteristics. Therefore, generating and receiving a millimeter wave signal is a challenge, but the biggest enemy with these high frequencies is the propagation media. The propagation characteristics and propagation loss of millimeter waves must be taken into account when the millimeter wave band technology is utilized as the backbone of future 5G cellular networks. A lower frequency spectrum can propagate for a longer distance, and can easily penetrate through buildings owing to its long wavelength. However, a millimeter wave which has a short wavelength can only propagate over a short distance, and cannot penetrate through solid materials very well [1, 2, 7].

Table 2.1 shows the attenuation level for some common materials [1, 2]. Certain building materials such as brick and concrete have high attenuation levels. They may keep the millimeter waves transmitted from the base station to be confined to streets and some other outdoor structures, although some of the signals may manage to reach inside the buildings through glass windows and wood doors which have low attenuation levels.

Table 2. 1 The attenuations level for different materials [1, 2]

Materials	Thickness (cm)	Attenuation (dB)		
		≤ 3 GHz	40 GHz	60 GHz
Drywall	2.5	5.4	-	6.0
Office whiteboard	1.9	0.5	-	9.6
Clear glass	0.3/0.4	6.4	2.5	3.6
Mesh glass	0.3	7.7	-	10.2
Chip wood	1.6	-	0.6	-
Wood	0.7	5.4	3.5	-
Plasterboard	1.5	-	2.9	-
Mortar	10	-	160	-
White wall	10	-	178	-
Concrete	10	17.7	175	-

In millimeter waves, the transmission loss is accounted for principally by the free space loss. However, the millimeter wave band also suffers from additional propagation losses such as the atmospheric absorption loss. Atmospheric absorption losses occur when the millimeter wave propagated through the mother earth are absorbed by water vapor, oxygen molecules, and other atmospheric gaseous[25]. At certain frequencies, the losses are higher, coinciding with the mechanical resonant frequencies of the gas molecules.

Figure 2.5 shows the atmospheric absorption losses at different frequencies across the millimeter-wave band. The blue circles show several peaks which the attenuation level is high due to the absorption of millimeter waves by atmospheric absorption. The green circles indicate frequencies with the attenuation level similar to the current communication systems. On the other hand, we can notice that the white colour circle shows the attenuation levels at 28 and 38 GHz (0.06 dB/km and 0.08 dB/km, respectively), which appear to be the lowest, providing the feasibility of millimeter-wave communication at such frequencies. For this reason, these frequencies are suitable candidates for future 5G cellular networks [8, 11, 26, 27].
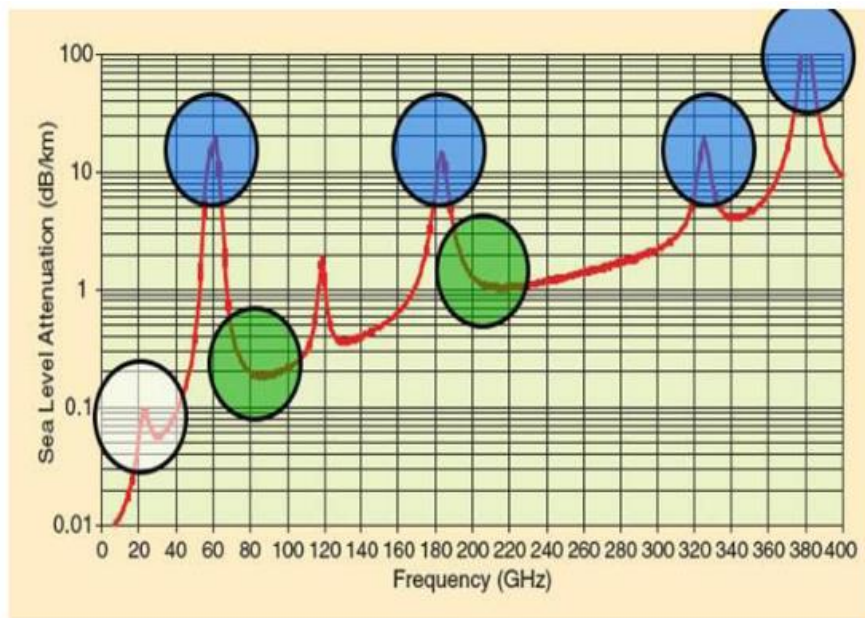
Figure 2. 5: The atmospheric absorption losses at different frequencies across the millimeter-wave band. [8, 11].

2.5 Skin Effect

The skin effect is defined as the tendency of electromagnetic wave energy to penetrate into the surface of a conductor only up to a certain depth [28, 29]. As shown in Figure 2.6, when an electromagnetic wave energy is transmitted along a conductor, the current flows only concentrate between the outer surfaces (circumference) to a level called '**skip depth**' of the conductor. This means that although the conductor may have a few inches of thickness, only the surface up to the skin depth of the conductor carries current. The current, electric field, and magnetic field decay exponentially with the distance from the circumference of the conductor.

Figure 2. 6: Skin depth of a conductor [29]

In short, the skin depth measures the deepness of the current, electric field, and magnetic field that can be penetrated into a conductor. It can be calculated by using the following equation [30]:

$$Skin\ Depth, \delta_s = \sqrt{\frac{2\rho}{2\pi f \mu_o \mu_r}} \quad (m) \qquad\qquad 2.1$$

where:

$\rho = bulk\ resitivity\ (\Omega.m)$

$f = frequency\ (Hz)$

$\mu_o = permeability\ of\ free\ space = 4\pi.10^{-7}(H/m)$

$\mu_r = relative\ magnetic\ permeability$

Based on Equation (2.1), we can observe that when the frequencies become higher, the skin depth shrinks. This indicates that at higher frequencies, the field is more difficult to penetrate into the surface of the conductor. Figure 2.7 shows a graph of skin depth versus frequency for some common conductors [30]. Notice that different materials of the conductor do not have a significant effect on the skin depth.
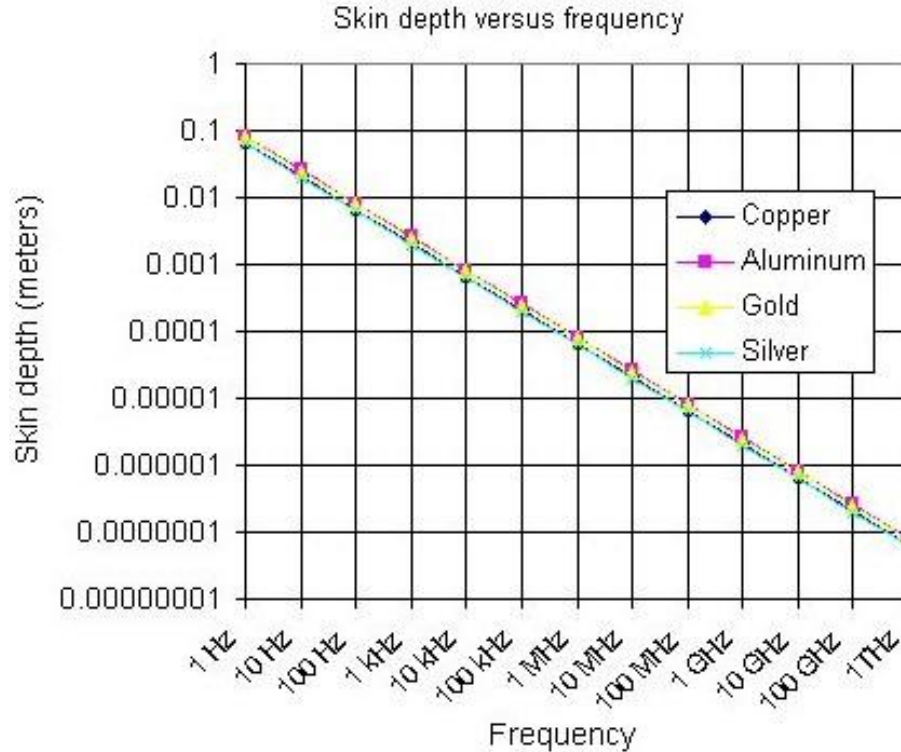
Figure 2. 7: A graph of skin depth versus frequency[30]

Increasing the applied frequency will lead to an increase in the inductive reactance of the conductor. Due to the high noise frequency, the charge is being pushed to the surface of the conductor [31], as shown in Figure 2.8. Overcrowded electrons at the surface of the conductor will experience an insufficient space to propagate, therefore increasing the friction among them. As a result, heat energy is produced and dissipated to the surrounding in the form of heat loss.

The flow of charge in the conductor when skin effects takes hold. Due to high frequency noise, the charge is being pushed to the circumference of the conductor.
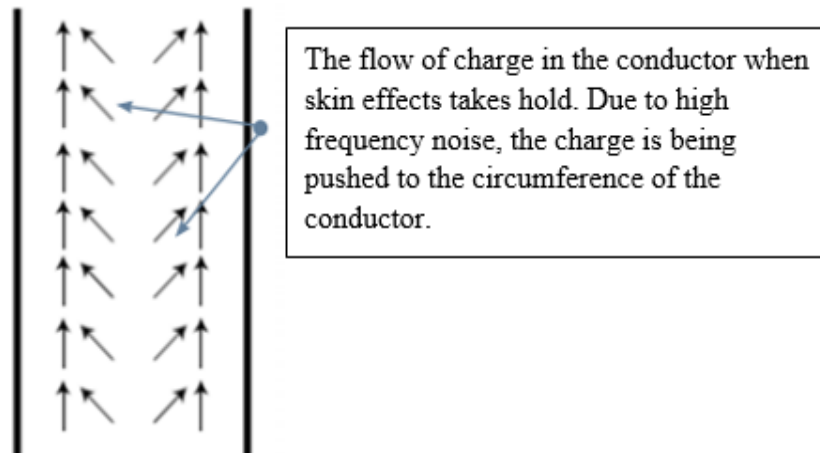
Figure 2. 8: The skin effects at high frequency noise [31]

14

In waveguides, the current flows along the inner surface of the guide. But, a waveguide consists of four walls for the current to propagate, increasing the total current-caring area as compared with other conductors such as coaxial cable and copper wire [32]. This allows the electrons to have more space to move, and less friction is produced. Therefore, a waveguide has a low level of loss due to the skin effect.

2.6 Chapter Summary

A literature review covering the scope of studies of this dissertation is presented in this chapter. Relevant publications that support the following discussion topics have been cited. Firstly, an introduction to waveguide theory is provided. Then, the differences between waveguide and TEM transmission line is analyzed and discussed. Next, the fundamental principles of TEM, TE, TM and hybrid waves and their corresponding propagation characteristics are summarized. Besides, the rectangular waveguide propagation mode and the skin effect are analyzed. Lastly, the millimeter wave propagation loss is discussed. The attenuation levels at 28 GHz is the lowest across the millimeter-wave band, providing the feasibility of millimeter-wave communication at this frequency for future 5G communication networks.

CHAPTER 3

METHODOLOGY

3.1 Research Methodology

A generalized research methodology has been followed in this dissertation to perform the iris waveguide bandpass filter design. Figure 3.1 depicts a flow chart pertaining to different phases of the waveguide bandpass filter design methodology adopted in this project. The activities in each phase of the design methodology are discussed in detail in this chapter.
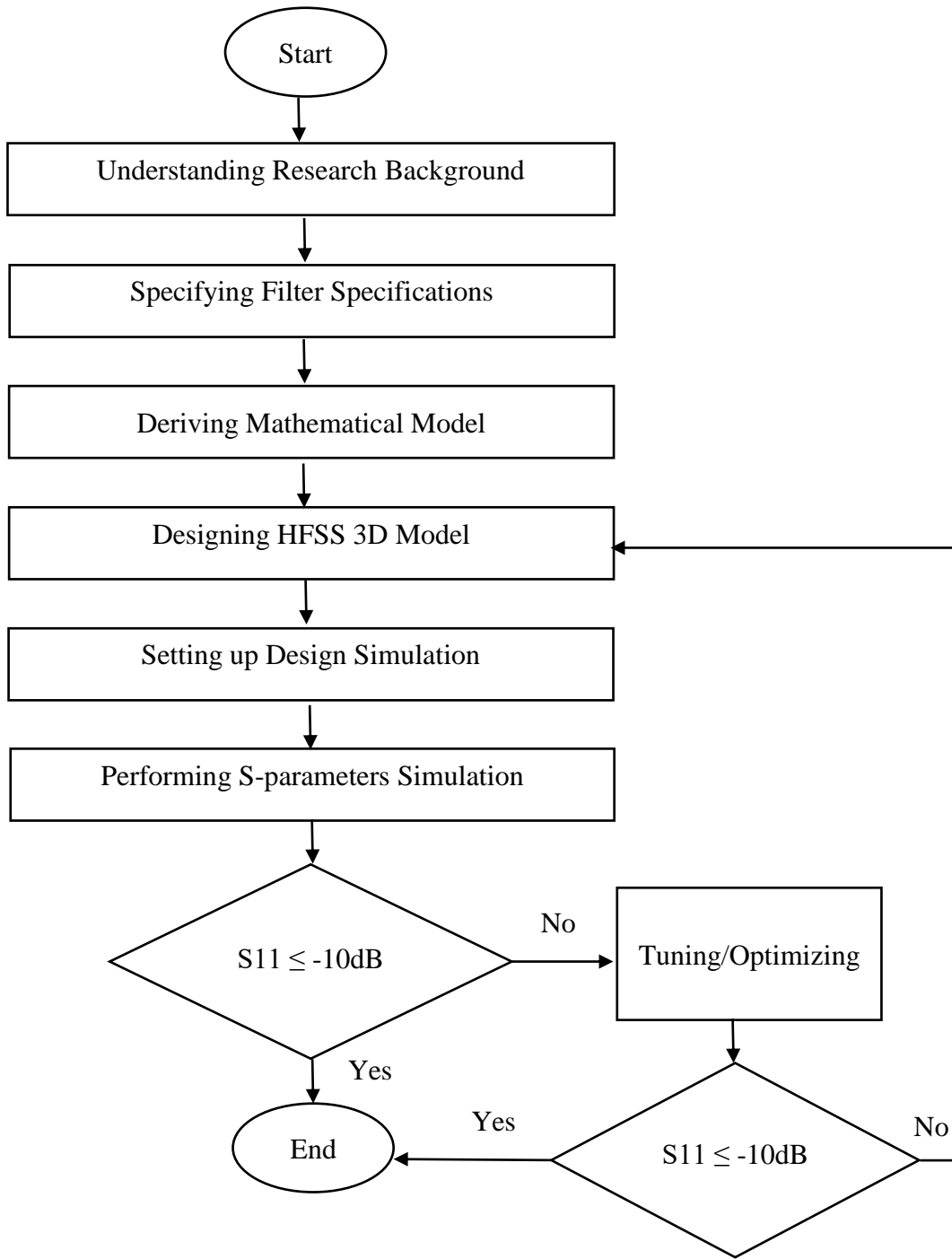
Figure 3. 1: The flow chart for the iris waveguide bandpass filter design methodology

3.1.1 Understanding Research Background

This project starts with a general study and understanding of future 5G cellular communication network technology and millimeter-wave frequency band. A lot of relevant information, which includes the theory of waveguide, Maxwell theorem, waveguide propagation mode, design techniques of bandpass waveguide filters, waveguide sizes and dimension, propagation losses of millimeter-wave, skin effects, has been gathered from various resources such as reference books, e-books, journals, conference papers and websites.

3.1.2 Specifying Filter Specifications

Based on the literature review pertaining to the background research, the propagation loss of millimeter-wave at 28 GHz is the lowest (0.06dB/km), proving the feasibility of millimeter-wave communication at this frequency. Therefore, the focus of this project is to design a WR-34 band (22-33GHz) millimeter-wave iris waveguide bandpass filter that operates at the center frequency of 28 GHz, with its relative bandwidth of 2.14%, ranging from 27.70 GHz to 28.30 GHz, to discriminate the wanted and unwanted signal frequencies for future 5G communication networks. The detailed design specifications of the filter are as follows:

Passband	27.70 GHz – 28.30 GHz
Return loss	$\geq$ 10dB
Stopband insertion loss	$\geq$ 40dB at 27.25 GHz
	$\geq$ 40dB at 28.75 GHz

The design must take the size and dimension of a rectangular waveguide into consideration as they determine the standard operating frequency range of the waveguide as well as other factors including attenuation level, mechanical size and weight, etc. A suitable waveguide enables a complete coverage of the frequency spectrum for a given application. Table 3.1 shows the rectangular waveguide standards and specifications.

Table 3. 1 The rectangular waveguide standards and specifications [33]

WR DESIGNATION	WG EQUIVALENT	STANDARD FREQ RANGE GHZ	INSIDE DIMENSIONS (INCHES)
WR284	WG10	2.60 - 3.95	2.840 x 1.340
WR229	WG11A	3.30 - 4.90	2.290 x 1.150
WR187	WG12	3.95 - 5.85	1.872 x 0.872
WR159	WG13	4.90 - 7.05	1.590 x 0.795
WR137	WG14	5.85 - 8.20	1.372 x 0.622
WR112	WG15	7.05 - 10.00	1.122 x 0.497
WR90	WG16	8.2 - 12.4	0.900 x 0.400
WR75	WG17	10.0 - 15.0	0.750 x 0.375
WR62	WG18	12.4 - 18.0	0.622 x 0.311
WR51	WG19	15.0 - 22.0	0.510 x 0.255
WR42	WG20	18.0 - 26.5	0.420 x 0.170
WR34	WG21	22.0 - 33	0.340 x 0.170
WR28	WG22	26.5 - 40.0	0.280 x 0.140
WR22	WG23	33 - 50	0.224 x 0.112
WR19	WG24	40 - 60	0.188 x 0.094
WR15	WG25	50 - 75	0.148 x 0.074
WR12	WG26	60 - 90	0.122 x 0.061

A suitable rectangular waveguide to meet the design specifications is the WR-34 band waveguide, with its operating frequency range from 22 to 33 GHz. The lowest order mode, TE10 cut-off frequency for the WR-34 band waveguide is 17.357 GHz, and its internal dimensions are 0.340 inches x 0.170 inches.

3.1.3 Deriving Mathematical Model

The next step is to derive with a mathematical model of the 28 GHz center frequency iris waveguide bandpass filter that meets the design specifications. This step is carried out by using a mathematical package, such as MATLAB or Maple.

The mathematical model derivation process commences by analyzing the level of ripple in the passband. The level of ripple, ε, can be determined by using the following formula [17]:

$$\varepsilon = \left(\frac{1}{1 - 10^{-\frac{LR}{10}}} - 1 \right)^{\frac{1}{2}} \qquad\qquad 3.1$$

where

LR = Return Loss in dB

The two guide wavelengths, $\lambda g1$ and $\lambda g2$, for the WR-34 waveguide can be determined using the following equation[17]:

$$\lambda g = \frac{\lambda}{\left(1 - \left(\frac{2\pi fc}{2\pi f} \right)^2 \right)^{\frac{1}{2}}} \qquad\qquad 3.2$$

where

f = Frequency

fc = Cut-off frequency of the waveguide

λ = Wavelength

c = Speed of light

The guide wavelength, $\lambda g0$, when the waveguide is half wavelength long can be calculated using [17]:

$$\lambda g0 = \frac{\lambda g1 + \lambda g2}{2} + \frac{1}{\pi} \left(\frac{\lambda g1 \cos\left(\frac{\pi \lambda g2}{2\lambda g1} \right) + \lambda g2 \cos\left(\frac{\pi \lambda g1}{2\lambda g2} \right)}{\sin\left(\frac{\pi \lambda g2}{2\lambda g1} \right) + \sin\left(\frac{\pi \lambda g1}{2\lambda g2} \right)} \right) \qquad\qquad 3.3$$

The attenuation constant, α, is obtained using [17]:

$$\alpha = \left(\frac{\lambda g1}{\lambda g0} \sin \left(\frac{\pi \lambda g0}{\lambda g1} \right) \right)^{-1} \qquad 3.4$$

The next step is to determine the required filter order, N. The filter order can be determined by analyzing the following insertion loss function, L [17] subject to different settings of N, whereby N is chosen to meet the most severe specification with respect to the insertion loss.

$$L = 10 \, log_{10} \left(1 + \varepsilon^2 T_n^{\,2} \left(\frac{\alpha \lambda g}{\lambda g0} \sin \left(\frac{\pi \lambda g0}{\lambda g} \right) \right) \right) \qquad 3.5$$

where

T_n is the Chebyshev Polynomials

Next, calculate the characteristics impedance of free space, η, as follows [17].

$$\eta \; = \; \sinh \left(\frac{1}{N} \sinh^{-1} \left(\frac{1}{\varepsilon} \right) \right) \qquad 3.6$$

The characteristic impedance, Z_r and characteristic admittance, $K_{r,r+1}$, values (normalized to 1 ohm) are then determined, as follows [17]:

$$Z_r = \frac{2\alpha}{\eta} \sin \left(\frac{(2r-1)\pi}{2N} \right)$$

$$- \frac{1}{4\eta\alpha} \left\{ \frac{\eta^2 + sin^2 \left(\frac{r\pi}{N} \right)}{\sin \frac{(2r+1)\pi}{2N}} + \frac{\eta^2 + sin^2 \left(\frac{(r-1)\pi}{N} \right)}{\sin \frac{(2r-3)\pi}{2N}} \right\} \qquad 3.7$$

with

$$z_0 = Z_{N+1} = 1 \qquad 3.8$$

for r = 1, … , N, and

$$K_{r,r+1} = \frac{\left(\eta^2 + \sin^2\left(\frac{r\pi}{N}\right)\right)^{\frac{1}{2}}}{\eta} \qquad 3.9$$

for r = 0, … , N.

The next step is to determine the respective susceptances of the inductive irises, $B_{r,r+1}$, by the following formula [17]:

$$B_{r,r+1} = \frac{(Z_{r,r+1})^{\frac{1}{2}}}{K_{r,r+1}} - \frac{K_{r,r+1}}{(Z_{r,r+1})^{\frac{1}{2}}} \qquad 3.10$$

for r = 0, … , N.

The phase lengths, ψ_r of the waveguide between irises are obtained, as follows[17]:

$$\psi_r = \pi - \frac{1}{2}\left[\cot^{-1}\left(\frac{B_{r-1,r}}{2}\right) + \cot^{-1}\left(\frac{B_{r,r+1}}{2}\right)\right] \qquad 3.11$$

for r = 1, … , N.

The physical lengths of the waveguides between irises, l_r are given by Equation 3.12 [17]. Each physical length is measured from the centerline of one iris to the centerline of the next.

$$l_r = \frac{\psi_r \lambda g0}{2\pi} \qquad 3.12$$

for r = 1, … , N.

The purely lumped-inductance discontinuities having shunt reactance, $X_{r,r+1}$, is given by [34]

$$\frac{X_{r,r+1}}{Z_0} = \frac{\dfrac{K_{r,r+1}}{Z_0}}{1 - \left(\dfrac{K_{r,r+1}}{Z_0}\right)^2} \qquad\qquad 3.13$$

for r = 0, … , N.

Lastly, the dimensions of the coupling irises are determined with the aid of chart in Figure 3.2.
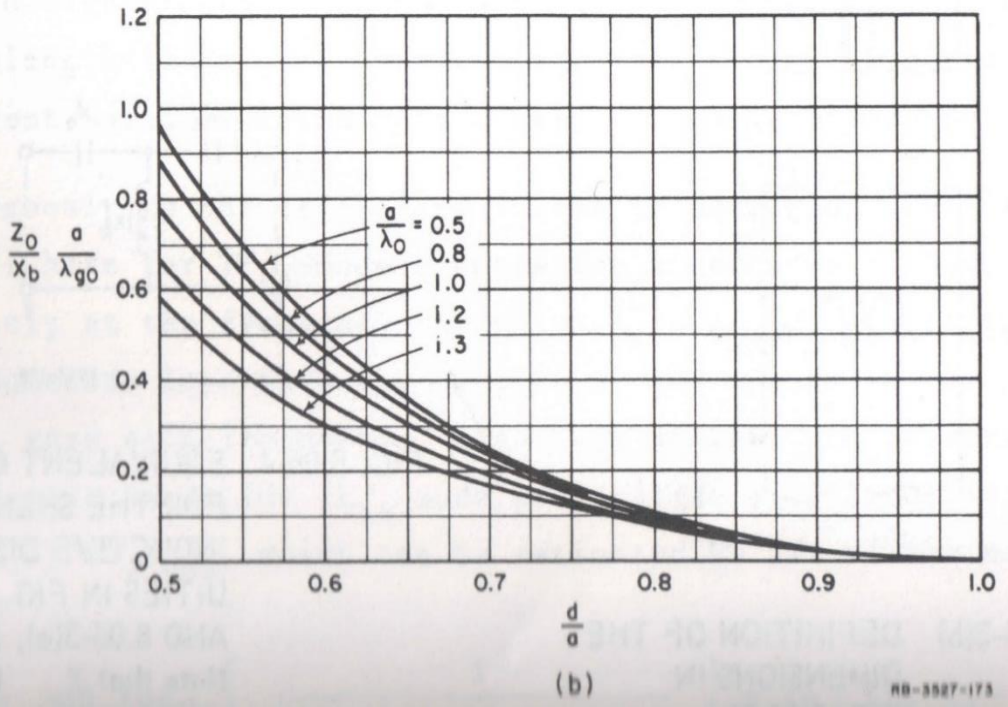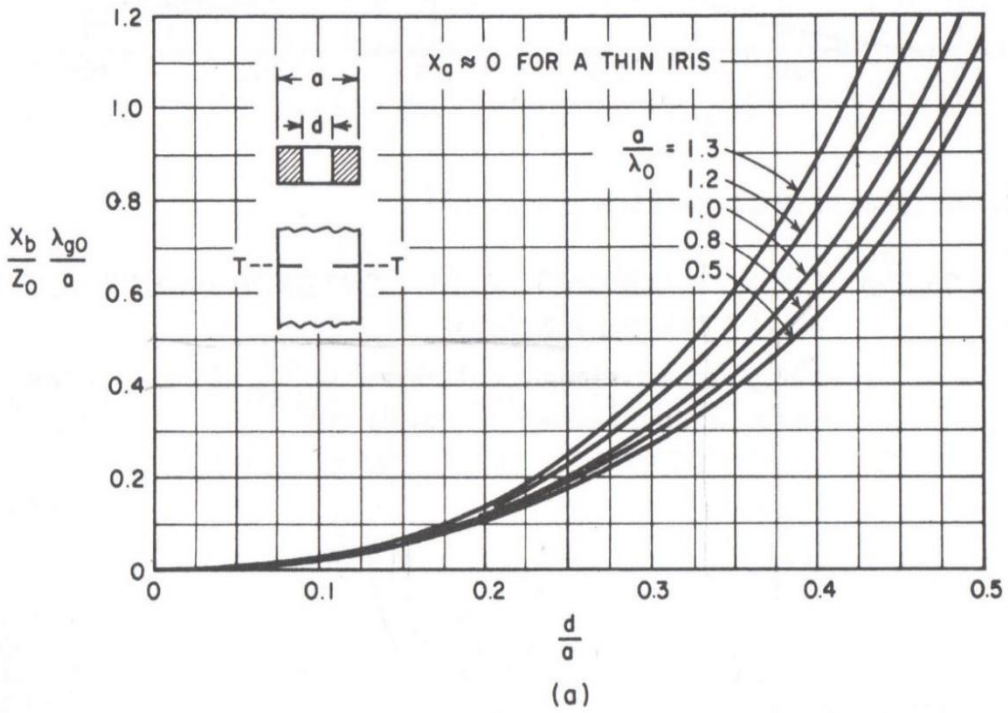
Figure 3. 2: Shunt reactance of symmetrical inductive window in rectangular waveguide [34]

3.1.4 HFSS Simulation

Learning the HFSS simulation software is an essential part of this project. It provides the necessary knowledge to formulate the 3D structure of the filter as well as to carry out the simulation and perform filter analysis. The mathematical model is validated by constructing a working simulation model using the HFSS simulation software to produce the desired outcome. The HFSS simulation steps include:

1. Designing HFSS 3D model
2. Setting up design simulation
3. Performing S-parameters simulation
4. Tuning and optimizing filter parameters

The details of each of the simulation steps will be discussed in Chapter 4.

3.2 Key Project Milestones

The project milestones mark the significant steps along the final year project timelines. The project milestones are important to ensure that the project progresses on-track according to the planned timelines.

3.2.1 Final Year Project 1 Milestones

Table 3.2 shows the milestones of final year project 1. The deliverables and due dates of the milestones are shown.

Table 3. 2 Milestones of Final Year Project 1

Milestone	Deliverable	Week
Research Background	• Learn future 5G technology and mm-wave band frequency • Understand waveguide theory, Maxwell theorem, bandpass filter design techniques, waveguide propagation mode and propagation losses, and related theories.	6
Mathematical Model Derivation	• Derive a mathematical model for waveguide bandpass filter	10
HFSS 3D Model Design	• Design and construct the 3D model waveguide bandpass filter based on the mathematical model	14

3.2.2 Final Year Project 2 Milestones

Table 3.3 shows the milestones of final year project 2. The deliverables and due dates of the milestones are listed.

Table 3. 3 Milestones of Final Year Project 2

Milestone	Deliverable	Week
Setup of Design Simulation	• Assign waveguide materials • Set up waveguide boundaries conditions • Set up excitation port	2
S-parameters Simulation	• Specify the simulation options • Validate the design setup • Create the S-parameters report • Analyze the filter response	7
Filter Parameter Tuning and Optimization	• Fine-tune and optimize the filter parameters to achieve the desired filter response.	10

3.3 Final Year Project Timeline (Gantt-Chart)

3.3.1 Final Year Project 1 Timeline

Table 3.4 shows the final year project 1 timeline. The completed activities are highlighted in green while the important due dates are highlighted in red.

Table 3. 4 Gantt chart of final year project 1

Activitity	Week													
	1	2	3	4	5	6	7	8	9	10	11	12	13	14
Selection of Project Topic	🟩	🟩												
Install Maple, ADS and HFSS Software		🟩												
Study the 5G Technology and Millimeter-wave Band Frequency			🟩	🟩	🟩									
Study the Basic Theory of Waveguides			🟩	🟩	🟩									
Study the Waveguide Bandpass Filter Design Technique			🟩	🟩	🟩									
Preparation for Extended Proposal					🟩									
Submission of Extended Proposal						🟥								
Waveguide Bandpass Filer Design						🟩	🟩	🟩						
Preparation for Proposal Defence									🟩					
Proposal Defence										🟥				
HFSS Software Learning											🟩	🟩		
3D Waveguide Bandpass Filter Construction in HFSS													🟩	🟩
Preparation for Interin Report													🟩	🟩
Submissionof Interim Draft Report													🟥	
Submission of Interim Report														🟥

3.3.2 Final Year Project 2 Timeline

Table 3.5 shows the final year project 2 timeline. The completed activities are highlighted in green while the important due dates are highlighted in red.

Table 3. 5 Gantt chart of final year project 2

Activitity	1	2	3	4	5	6	7	8	9	10	11	12	13	14	15
Bandpass Filter Simulation and Fine Tuning by HFSS	�	▩	▩	▩	▩	▩	▩	▩	▩	▩					
Preparation for Progress Report						▩									
Submission of Progress Report							▧								
Pre-SEDEX Preparation								▩	▩						
Pre-SEDEX										▧					
Preparation for Fianl Report											▩	▩	▩		
Submission of Draft Final Report													▧		
Preparation for Dissertation											▩	▩	▩		
Submission of Dissertation (soft bound)														▧	
Preparation for Technical Paper											▩	▩	▩		
Submission of Technical Paper														▧	
Preparation for Viva Presentation											▩	▩	▩	▩	
Viva															▧
Submission of Project Dessertation (Hard Bound)															▧

3.4 Chapter Summary

A generalized research methodology to perform the iris waveguide bandpass filter design is presented. The activities in each phase of the design methodology are explained in detail. Besides that, the key project milestones and the corresponding Gantt chats of final year projects 1 and 2 are included.

CHAPTER 4

RESULTS AND DISCUSSION

4.1 Theoretical Design of the Iris Waveguide Bandpass Filter

In this project, the aim is to design a rectangular waveguide bandpass filter that satisfies with the specifications in Table 4.1.

Table 4. 1 Rectangular waveguide bandpass filter specifications

Filter Parameter	Specification
Centre Frequency	28 GHz
Passband Range	27.70 GHz to 28.30 GHz
Lower Passband Frequency (fp1)	27.70 GHz
Upper Passband Frequency (fp2)	28.30 GHz
Lower Stopband Frequency (fs1)	27.25 GHz
Upper Stopband Frequency (fs2)	28.75 GHz
Lower Stopband Insertion Loss (LA1)	≥ 40 dB
Upper Stopband Insertion Loss (LA2)	≥ 40 dB
Passband Return Loss (LR)	≥ 10 dB

Based on the specifications in Table 4.1, the ripple level of the waveguide bandpass filter is determined using Equation 3.1, which yields

$\varepsilon = 0.100$

The two guide wavelengths, λg1 and λg2, for the WR-34 waveguide are determined using Equation 3.2, which yields

λg1 = 0.01389686557 m

λg2 = 0.01342144788 m

The guide wavelength, λg0, when the waveguide is half wavelength long is calculated using Equation (3.3), which yields

λg0 = 0.01365916085 m

From Equation (3.4), the attenuation constant, α, is determined, i.e.,

α = 18.29975928

The required filter order, N, is then determined by using Equation 3.5, subject to different N settings. When N = 1, we have

$$T_1(x) = x \qquad\qquad 4.1$$

Substituting $T_1(x)$ into Equation 3.2 gives the filter frequency response shown in Figure 4.1.
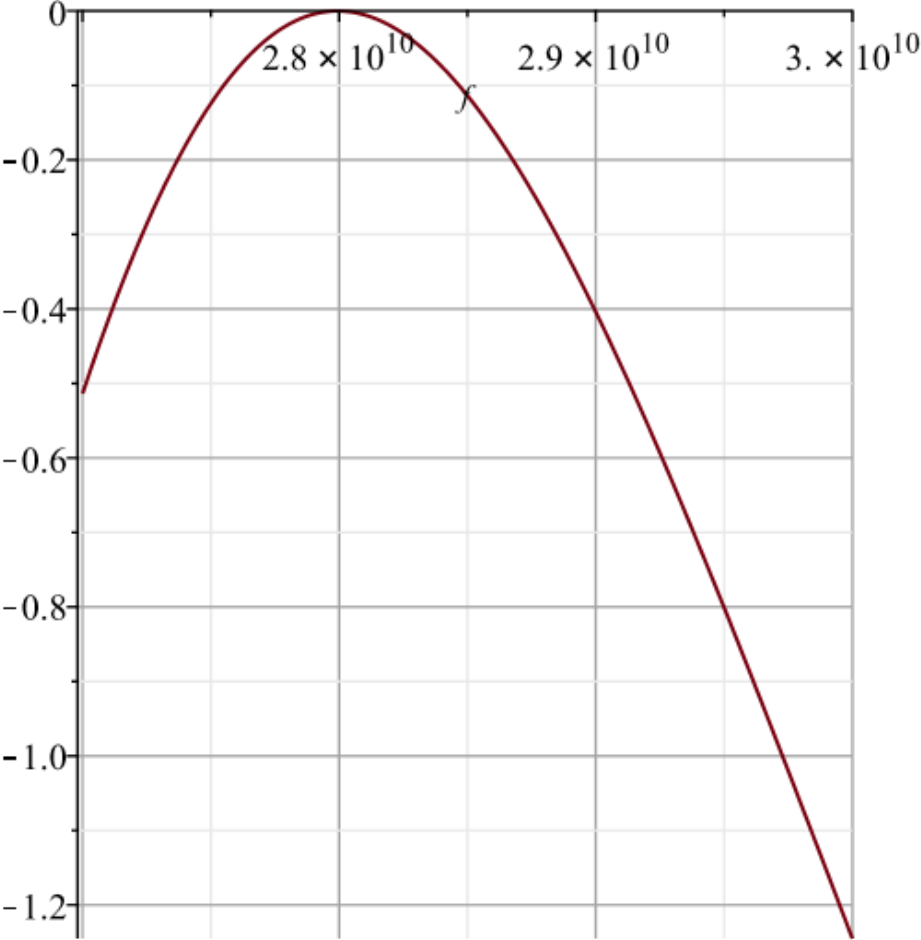
Figure 4. 1: The filter frequency response when N=1

When N = 2, we have

$$T_2(x) = 2x^2 - 1 \qquad\qquad 4.2$$

Substituting $T_2(x)$ into Equation 3.2 gives the gives the filter frequency response shown in Figure 4.2.
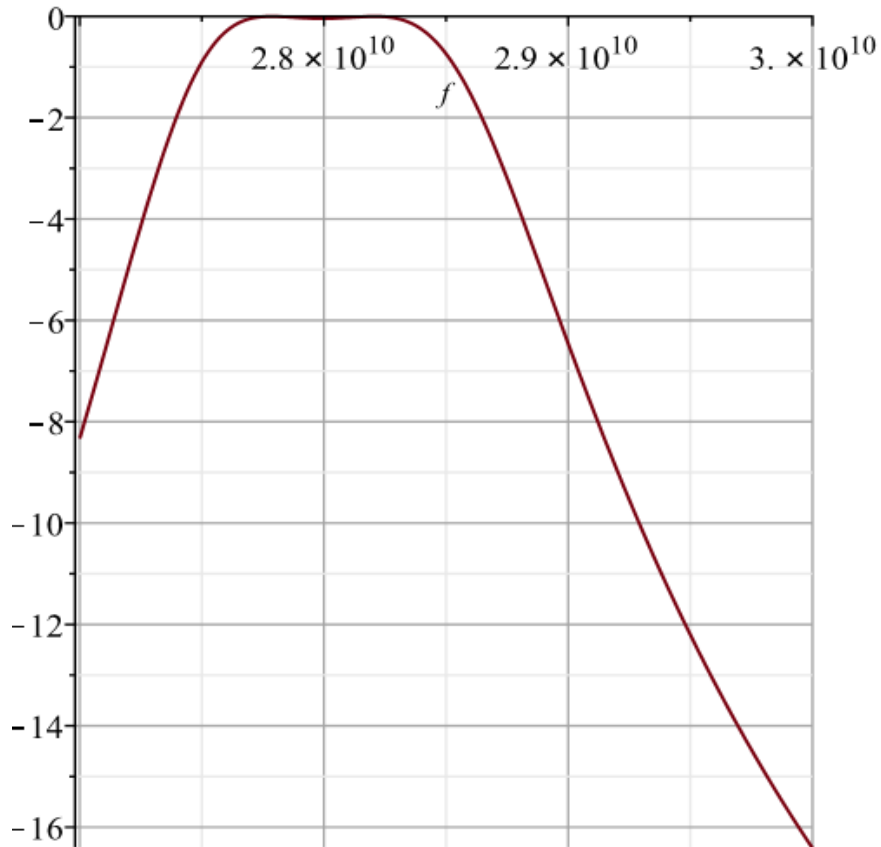
Figure 4.2: The filter frequency response when N=2

When N = 3, we have

$$T_3(x) = 4x^3 - 3x \qquad\qquad 4.3$$

Substituting $T_3(x)$ into Equation 3.2 gives the filter frequency response shown in Figure 4.3.
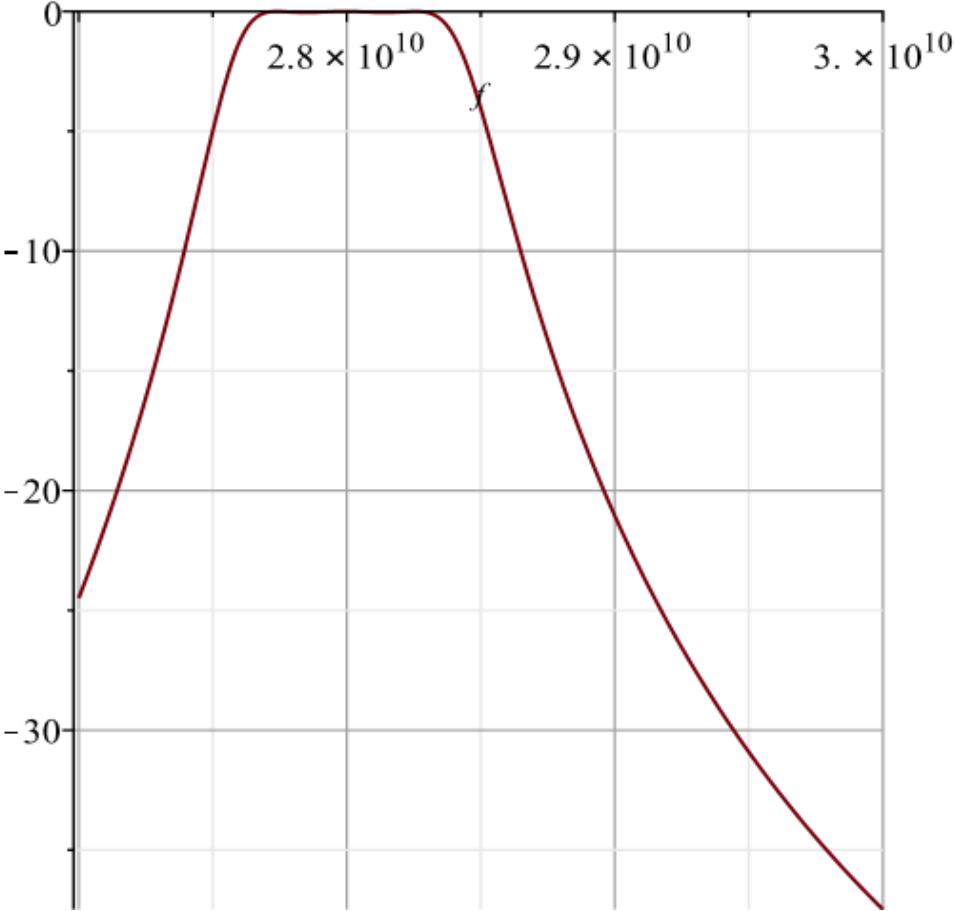
Figure 4. 3: The filter frequency response when N =3

When N = 4, we have

$$T_4(x) = 8x^4 - 8x^2 + 1 \qquad\qquad 4.4$$

Substituting $T_4(x)$ into Equation 3.2 gives the filter frequency response shown in Figure 4.4.
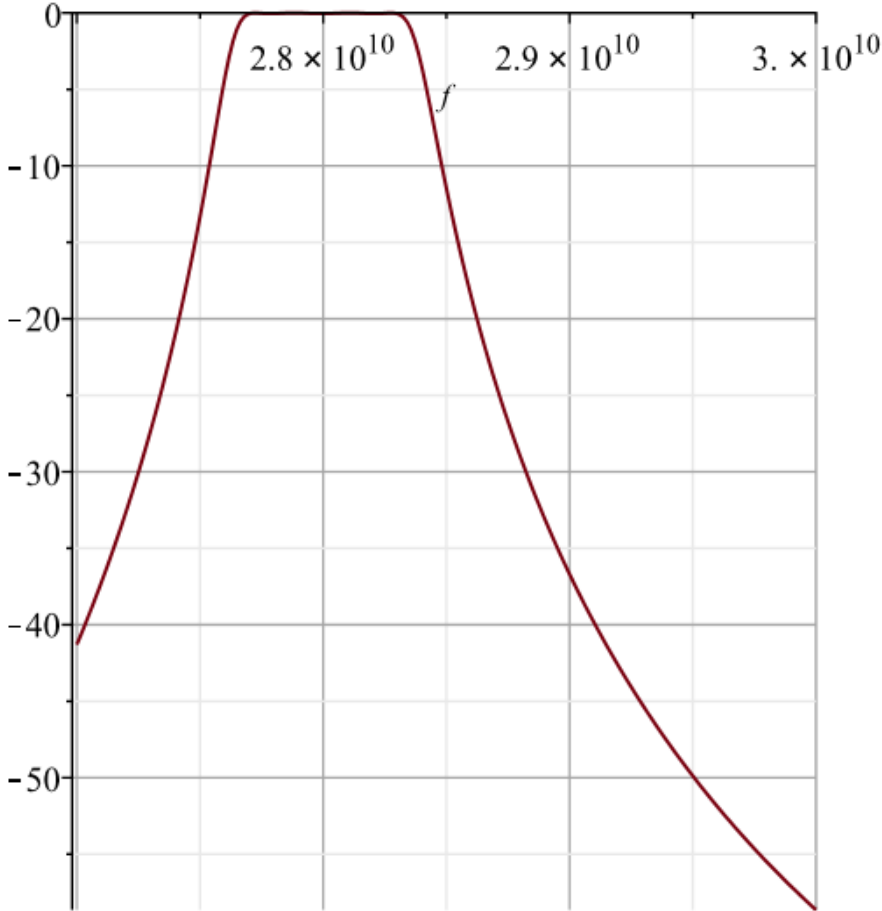
Figure 4. 4: The filter frequency response when N = 4

When N = 5, we have

$$T_4(x) = 16x^5 - 20x^3 + 5x \qquad\qquad 4.5$$

Substituting $T_5(x)$ into Equation 3.2 gives the filter frequency response shown in Figure 4.5.
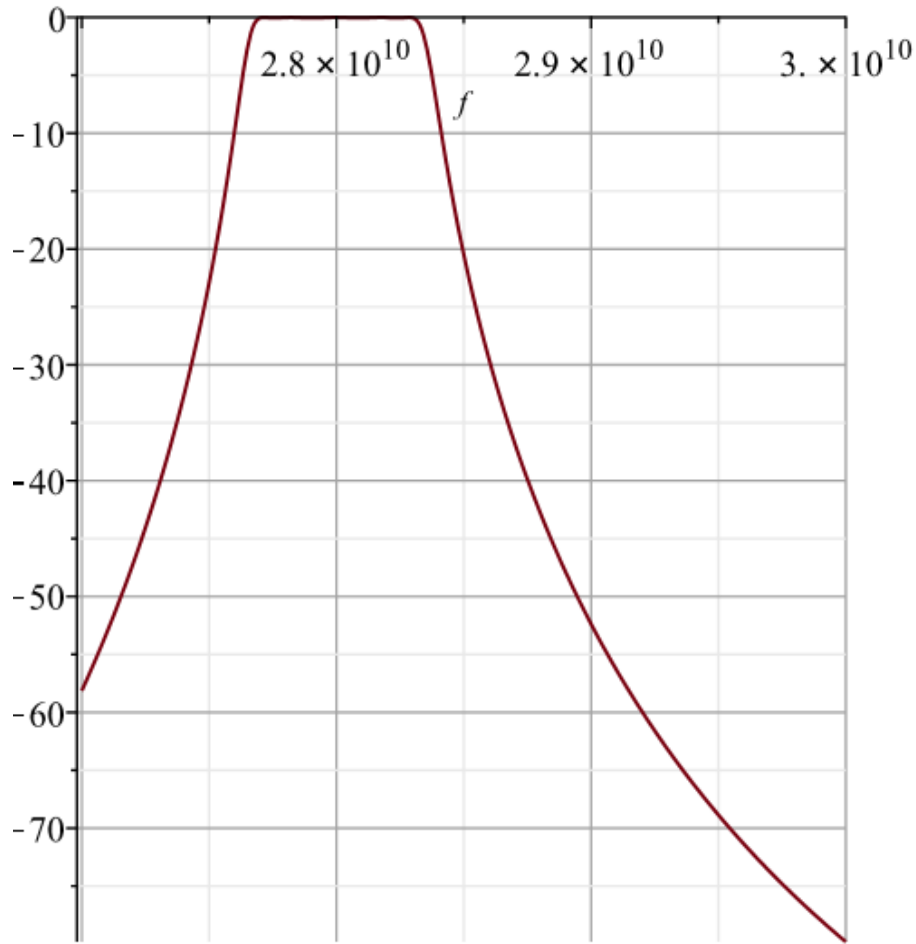
Figure 4. 5: The filter frequency response when N =5

From Figure 4.5, when N=5, notice that the stopband insertion loss is ≤ -40dB at 27.25 and 28.75 GHz, respectively. This response meets the filter specifications, i.e., satisfying the most severe specification with respect to the insertion loss. Therefore, the required filter order is N = 5.

Having determined N=5, the characteristic impedance, Z_r, and characteristic admittance, $K_{r,r+1}$, values (normalized to 1 ohm) are determined using Equations 3.6 to 3.9, which yields

$Z_1 = Z_5 = 17.78454066$

$Z_2 = Z_4 = 46.45878000$

$Z_3 = 57.45590104$

$K_{01} = K_{56} = 1.00$

$K_{12} = K_{45} = 1.361434818$

$K_{23} = K_{34} = 1.798472818$

The susceptances of the inductive irises, $B_{r,r+1}$, are determined using Equation 3.10, which yields

$B_{01} = B_{56} = 3.980046390$

$B_{12} = B_{45} = 21.06604636$

$B_{23} = B_{34} = 28.69265762$

The phase lengths, ψ_r, of the waveguide between irises are then obtained using Equation 3.11, which yields

$\psi_1 = \psi_5 = 2.861439277$

$\psi_2 = \psi_4 = 3.059468918$

$\psi_3 = 3.072000973$

The physical lengths, l_r, of the waveguides between irises are calculated using Equation 3.12, which yields

$l_1 = l_5 = 0.622$ cm

$l_2 = l_4 = 0.665$ cm

$l_3 = 0.667$ cm

Lastly, the dimensions of the coupling irises are determined with the aid of the chart in Figure 3.2, giving

$d0 = d6 = 0.292$ cm

$d1 = d4 = 0.144$ cm

$d2 = d3 = 0.125$ cm

The filter design parameters are summarized in Table 4.2, while the waveguide filter circuit diagram is shown in Figure 4.6.

Table 4. 2 The theoretical filter design parameters

Design Parameter	Theoretical Value
$d0$	0.292 cm
$d1$	0.144 cm
$d2$	0.125 cm
$d3$	0.125 cm
$d4$	0.144 cm
$d5$	0.292 cm
l_1	0.622 cm
l_2	0.665 cm
l_3	0.667 cm
l_4	0.665 cm
l_5	0.622 cm
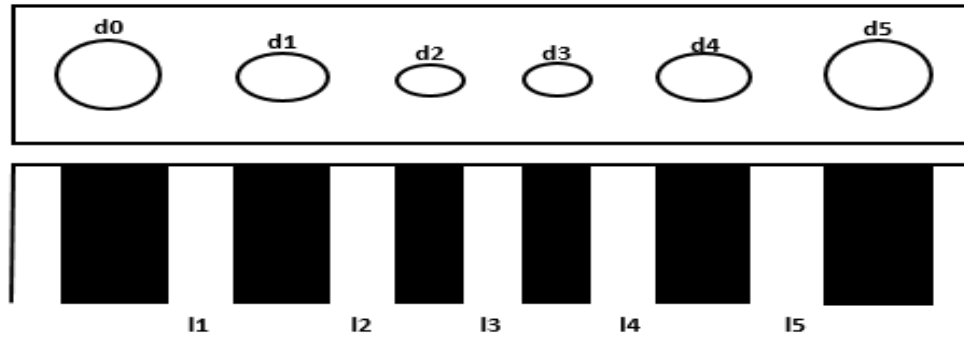
Figure 4. 6: The waveguide filter circuit diagram

4.2 Simulation of a Waveguide Bandpass Filter Prototype Using HFSS

4.2.1 Creating New Project

The simulation procedure starts with creating a new project, which saves all the data associated with the waveguide bandpass filter prototype.   Click on **Project > Insert HFSS Design.** A 3D modeler window appears on the screen, as shown in Figure 4.3. The green, red and blue lines in the HFSS 3D Modeler window represent the x, y and z axes, respectively.
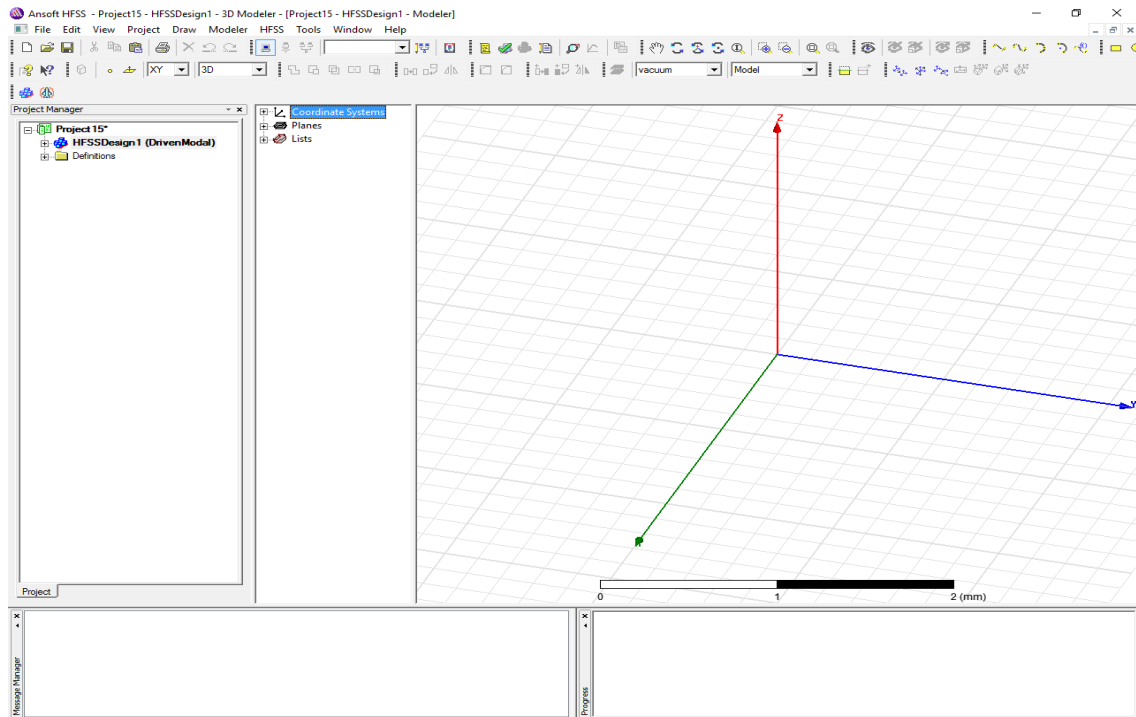
Figure 4. 7: The HFSS 3D modeler window

4.2.2 Selecting the HFSS Solution Type

To set the solution type, click on **HFSS > Solution Type**. The solution type window appears on the screen, as shown in Figure 4.4. Select the Driven Model for the solution type for the filter prototype. The Driven Model is used to calculate the model based on S-parameters "driven" by a source. The S-matrix solution is expressed in terms of the incident and reflected powers of the waveguide model.
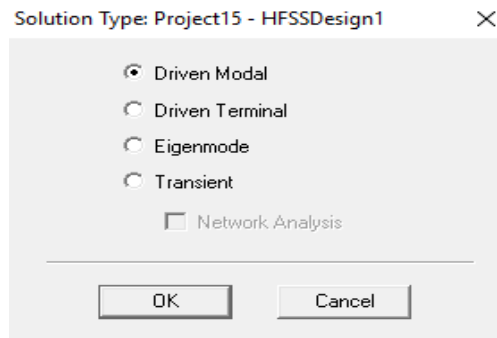
Figure 4. 8: The HFSS solution type window

4.2.3 Setting the Measuring Unit of the Waveguide Model

To set the model measuring unit, go to **Modeler > Unit.** The "Set Model Units" window appear on the screen, as shown in Figure 4.5. The waveguide measuring unit should be in mm.
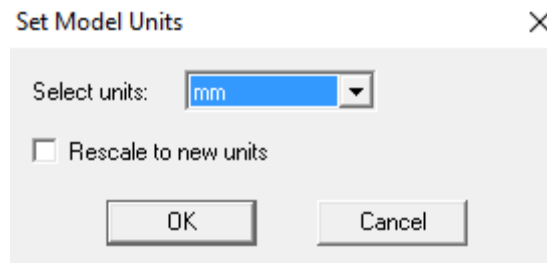
Figure 4. 9: The HFSS set model units window

4.2.4 Creating the Waveguide 3D Model

To draw the rectangular waveguide, go to the "Draw" Menu and click on "Box". The first object that needs to be drawn is the hollow tube of the rectangular waveguide. The hollow tube of the waveguide can be drawn by specifying the staring position of the box, which is followed by entering the X-Size, Y-Size, and Z-Size of the box, respectively. In this project, WR-34 is chosen with the inner dimension of 8.636mm x 4.318mm. These values represent the X-Size and Y-Size, respectively. For the Z-Size, a random number is assigned as the final Z-Size of the waveguide is not fixed yet, and will be determined later

during the optimization step. Figure 4.6 shows the properties window for the coordinates and size of the box.

	Name	Value	Unit	Evaluated Value	Description	
	Command	CreateBox				
	Coordinate Sys...	Global				
	Position	0 ,0 ,0	mm	0mm , 0mm , 0mm		
	XSize	$a		0.00864		
	YSize	$b		0.00432		
	ZSize	$L		0.0464623625		
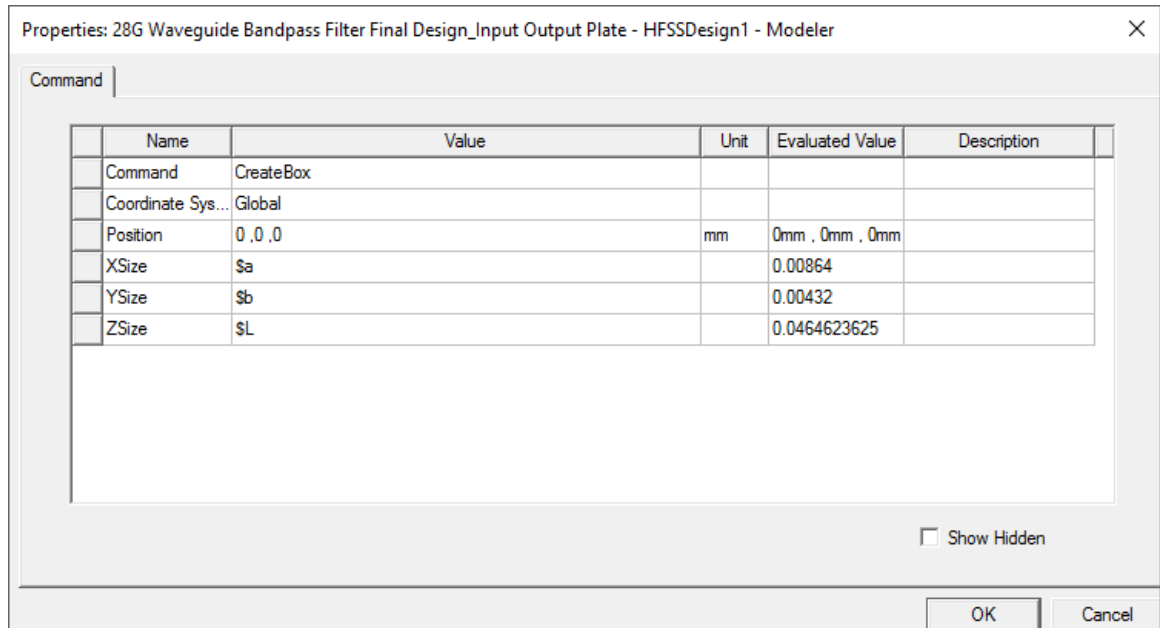
Figure 4. 10: The properties window for the coordinates and size of the box

The next step is to draw the conductive tube of the rectangular waveguide. Follow the same step as mentioned above, but with the conductive tube of the waveguide slightly bigger than the hollow tube of the waveguide. After that, go to **Modeler > Boolean > Substrate** to substrate the hollow tube from conductive tube of the rectangular waveguide. This is to ensure that the rectangular waveguide structure consists of a conducting wall with a uniform cross-section hollow center. Figure 4.7 shows the 3D structure of the rectangular waveguide in HFSS.
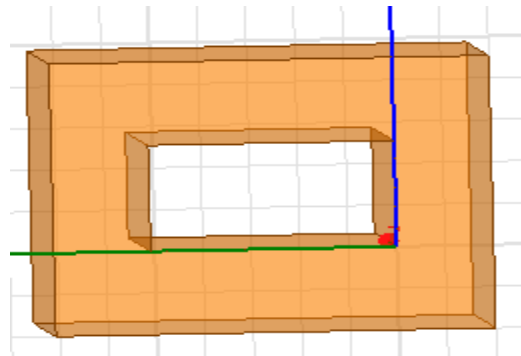
Figure 4. 11: The 3D structure of a rectangular waveguide in HFSS

Lastly, the posts that act as shunt inductive discontinuities connected across the broad wall of the guide need to be drawn. Go to the "Draw" menu and click on "Cylinder" to draw the posts. A total of 6 posts are required based on the derived mathematical model. The lengths between each post and the diameter of every other post are specified by following the derived mathematical model in Table 4.2. The height of all the posts is 8.64mm (height of the guide). The final 3D structure of the waveguide bandpass filter with irises is shown in Figure 4.8.
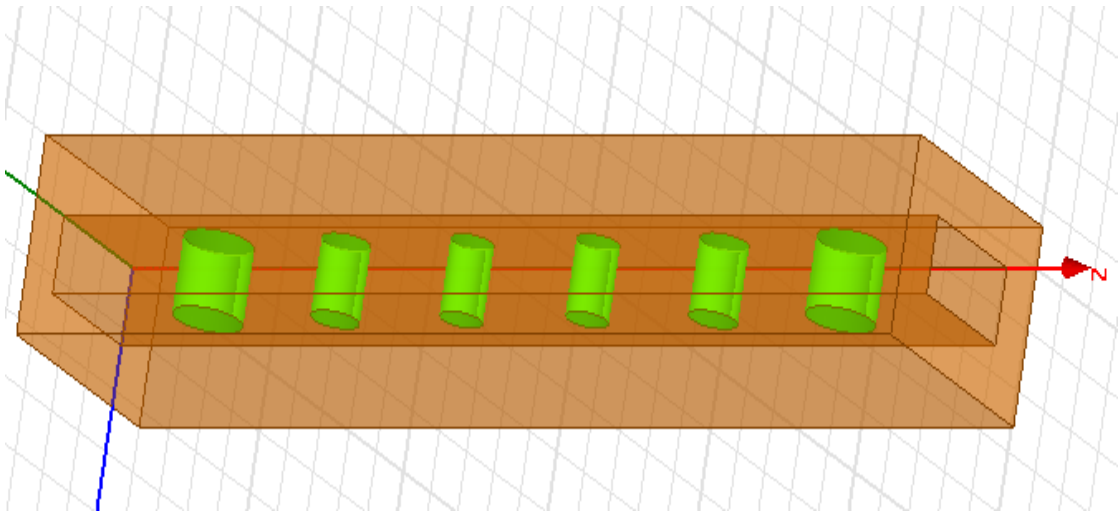
Figure 4. 12: The 3D structure of the bandpass filter with irises

4.2.5 Assigning the Waveguide Materials

After completing the 3D modelling, right click on the 3D waveguide model to access the 3D Modeler menu. Select "Assign Material" and a Select Definition window appears, as shown in Figure 4.9. Assign "Aluminum" for both the conducting wall and the irises of the waveguide, while assign "Air" for the hollow tube of the guide.
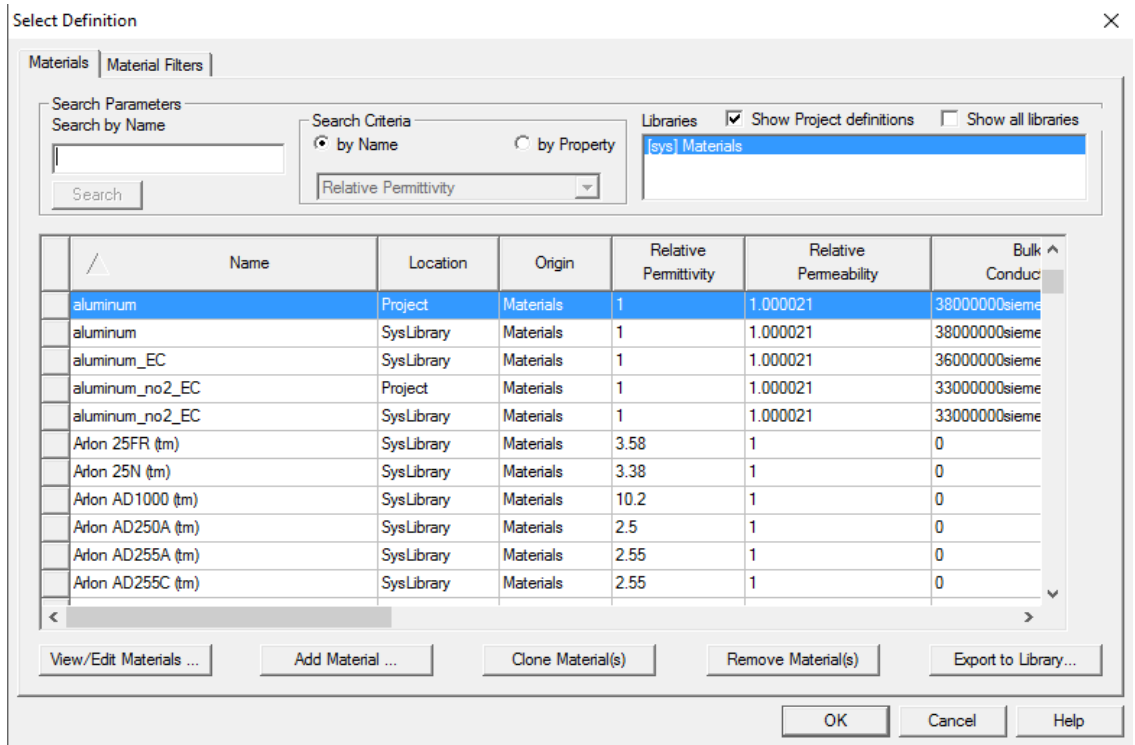
Figure 4. 13: The Select Definition window

4.2.6 Setting the Boundary Conditions

The objective of setting the boundary conditions is to specify the guide field behavior at the edges of the problem region and object interfaces. The Perfect E category should be assigned to the 3D waveguide structure expect the hollow tube. Go to **HFSS > Boundaries > Assign > Perfect E.**

4.2.7 Setting the Excitation Port

A wave port is the surface where the signals enter and leave the guide. Right click on the 3D Modeler Window and activate "Select Faces". In the Select Faces Mode, right click on the cross-section area of the hollow tube, and go to **Assign Excitation > Wave Port.** In the **Wave Port: General** step, key in the wave port name and click "**Next**". For this project, the number of modes required is 1, therefore one wave port integration line must be drawn from the middle bottom of the cross-section area of the hollow tube to the

top, as shown in Figure 4.10. Next, another wave port needs to be assigned at the other end of the guide. The same steps are followed.
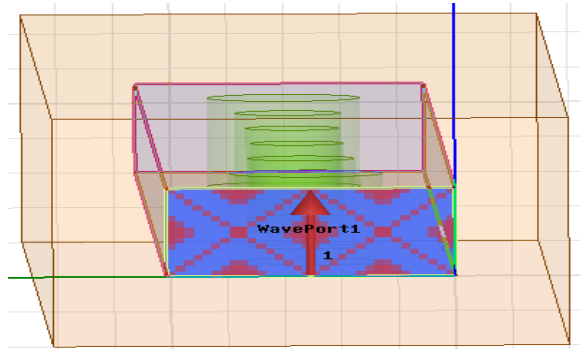
Figure 4. 14: Assigning the waveguide wave port

4.2.8 Generating a Solution

A solution setup is added in order to specify how the software will compute the solution. This step can be accomplished by going to **HFSS > Analysis Setup > Add Solution Setup**. A Solution setup window appears. Set the Solution Frequency to 28 GHz, and accept all other default settings. After that, go to **HFSS > Analysis Setup > Add frequency Sweep.** An "Edit Sweep" dialog appears, as shown in Figure 4.11. The frequency sweep should start from 25GHz and end at 31 GHz, since the waveguide center frequency is at 28GHz.
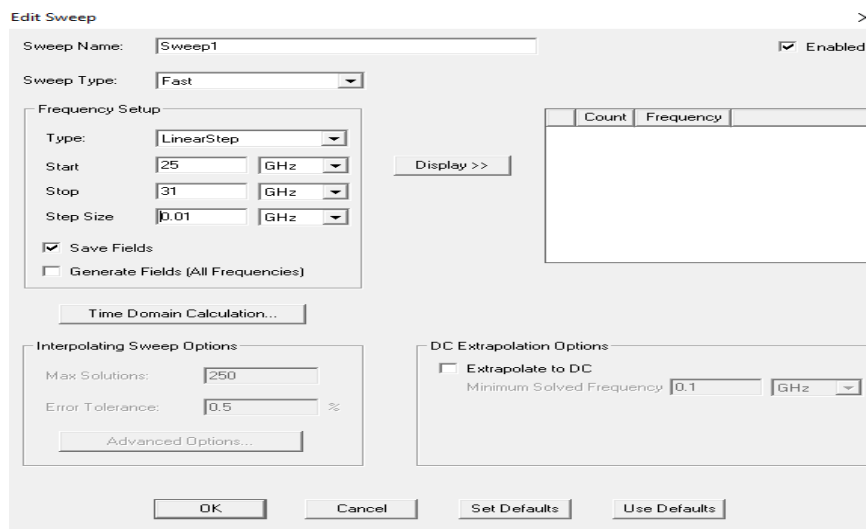
Figure 4. 15: The Edit Sweep dialog box

4.2.9 Validation Check and Simulation Run

Next, move on to the validation check. This step can be accomplished by accessing **HFSS > Validation Check.** A validation check window appears on the screen, as shown in Figure 4.12. If there is no error in the validation check, it is ready to run the simulation. Go to **HFSS > Analyze All** to run the simulation.
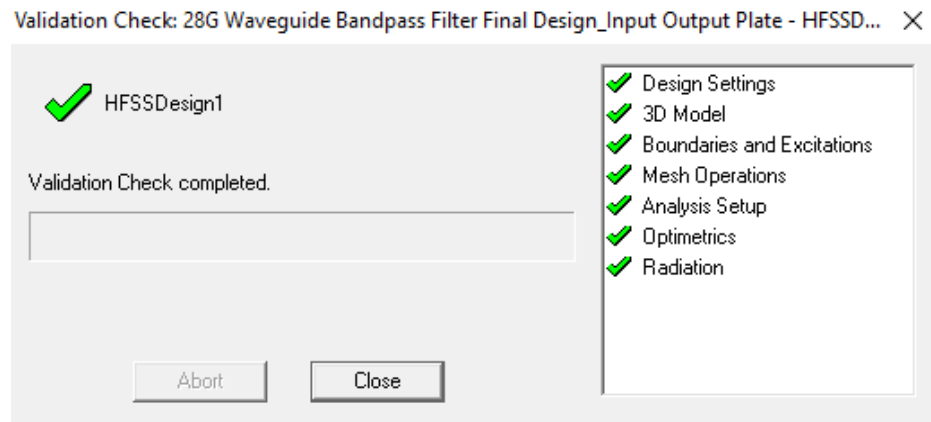
Figure 4. 16: The HFSS validation check window

4.2.10 Tuning and Optimization

Tuning refers to the process of adjusting all the filter parameters to yield the desired filter response. Tuning screws are added to the waveguide filter. Specifically, there are 6 inductive posts and 7 tuning screws. The tuning screws are added to the center of each inductive post, including one before and one after the inductive post. Each tuning screw acts like an inductive post, but it does not have an end-to-end touch of the guide. For the initial design, the diameter of the tuning screw is set to 0.3 cm, and the protruding length is set to 0.05 cm. Figure 4.13 depicts the 3D structure of the designed waveguide bandpass filter, together with all the tuning screws. The inductive posts are in blue while the tuning screws are in green. All the filter parameters are tuned empirically, in order to produce the filter response as close as possible to the desired specification.
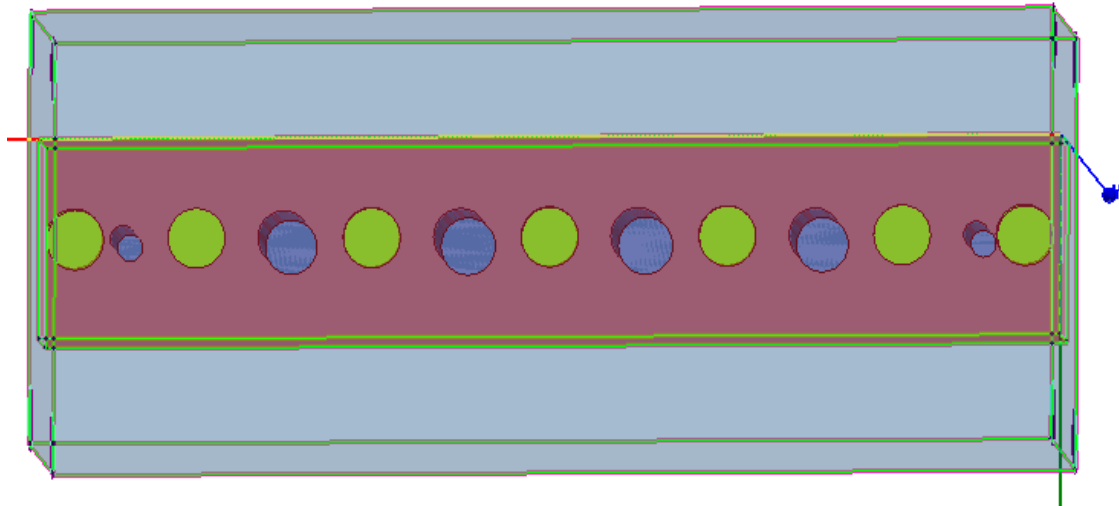
Figure 4. 17: The 3D structure of the waveguide bandpass filter with inductive posts and tuning screws

Next, the HFSS optimization engine is used to perform parametric analysis, sensitivity analysis, and optimization of all filter parameters to produce the desired filter response. This step can be accomplished by accessing **HFSS > Optimetrics Analysis > Add Optimization**. A setup optimization window appears on screen as shown in Figure 4.14. Moving on, select the 'Pattern Search' algorithm as the optimizer. The goal and condition are set according to the filter specifications.

Figure 4. 18: The Setup optimization window

In the **Variables** tab, select and include all the filter parameters for the optimization process. The filter parameters optimization range is set as shown in Figure 4.15. A total of 12 filter parameters exist, and the HFSS simulation software adjusts the filter parameters automatically to produce the best filter response.

Setup Optimization													✕

Goals | Variables | General | Options

Variable	Override	Starting Value	Units	Include	Min	Units	Max	Units	Min Step	Units	Max Step	Un
$D	✔	2.2838	m	✔	0.01	m	10	m	0	m	0.1	m
$D0	✔	1.12646	m	✔	0.01	m	10	m	0	m	0.1	m
$D1	✔	2.285885	m	✔	0.01	m	10	m	0	m	0.1	m
$D2	✔	2.52274	m	✔	0.01	m	10	m	0	m	0.1	m
$L1	✔	5.66829	m	✔	0.01	m	10	m	0	m	0.1	m
$L2	✔	5.63935	m	✔	0.01	m	10	m	0	m	0.1	m
$L3	✔	5.6046875	m	✔	0.01	m	10	m	0	m	0.1	m
$X	✔	4.45951	m	✔	0.01	m	10	m	0	m	0.1	m
$h1	✔	0.529265	m	✔	0.01	m	10	m	0	m	0.1	m
$h2	✔	0.0703125	m	✔	0.01	m	10	m	0	m	0.1	m
$h3	✔	0.297431	m	✔	0.01	m	10	m	0	m	0.1	m
$h4	✔	0.353222	m	✔	0.01	m	10	m	0	m	0.1	m

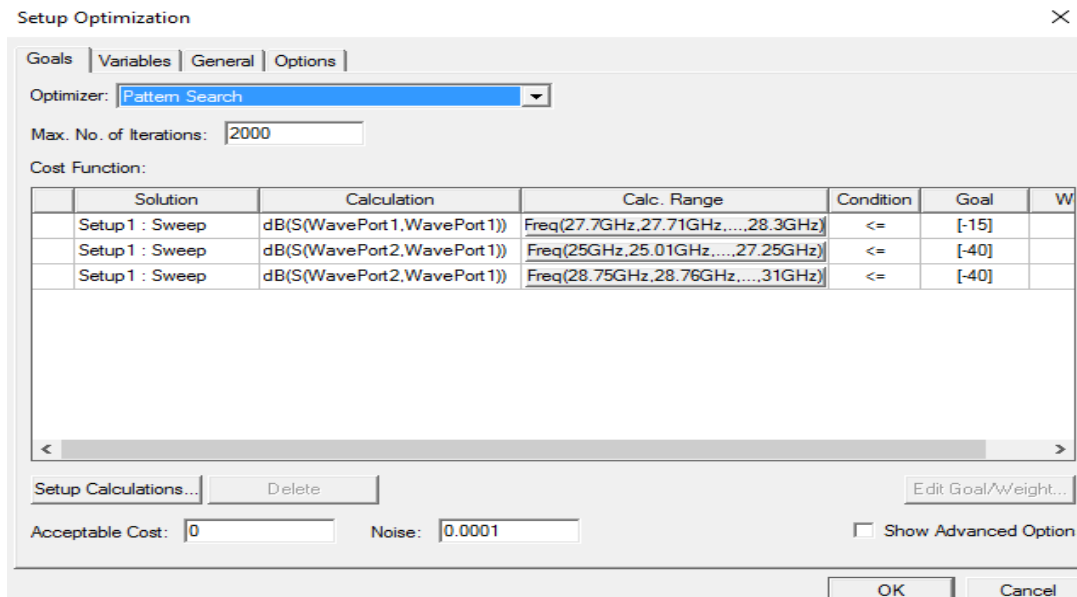Set Fixed Variables...   Linear Constraint...

OK | Cancel

Figure 4. 19: The setup of the filter parameter optimization range

The final optimized filter parameters, including the tuning screws design parameters are as follows: d0=d5=1.145mm, d1=d4=2.358cm, d2=d3=2.479mm, $l_1 = l_5 = 5.572$mm, $l_2 = l_4 = 5.624mm$, $l_3 = 5.582$ mm, h1=h7=0.648mm, h2=h6=0.025mm, h3=h5=0.279mm, h4=0.341mm, L= 464.62mm, th=5mm, X=3.2624mm and D=2.59mm, where parameter h is the height of the tuning screws, L is the length of the waveguide, D is the diameter of the tuning screws, th represents the thickness of the conductive tube and X is the length before and after the first and last inductive post from the wave port.

4.2.11 S-parameters Simulation Results

The S-parameter simulation results are shown in Figure 4.16. The results depict that the center frequency of the filter is at 27.995 GHz. The lower stopband frequency (fp1) is 27.71 GHz while the upper stopband frequency (fp2) is 28.28 GHz. Therefore, the passband ranges from 27.71 GHz to 28.28 GHz, with a relative bandwidth of 2.03%. The return loss for the entire passband is better than 7.8dB. The S-parameters simulation results also indicate that the filter has an upper and lower stopband insertion loss measurements of better than 40dB at 27.25 GHz and 28.75 GHz, respectively. This filter can achieve a 570 MHz bandwidth with S11 ≤ -7.8 dB and S21 ≤ 1dB.

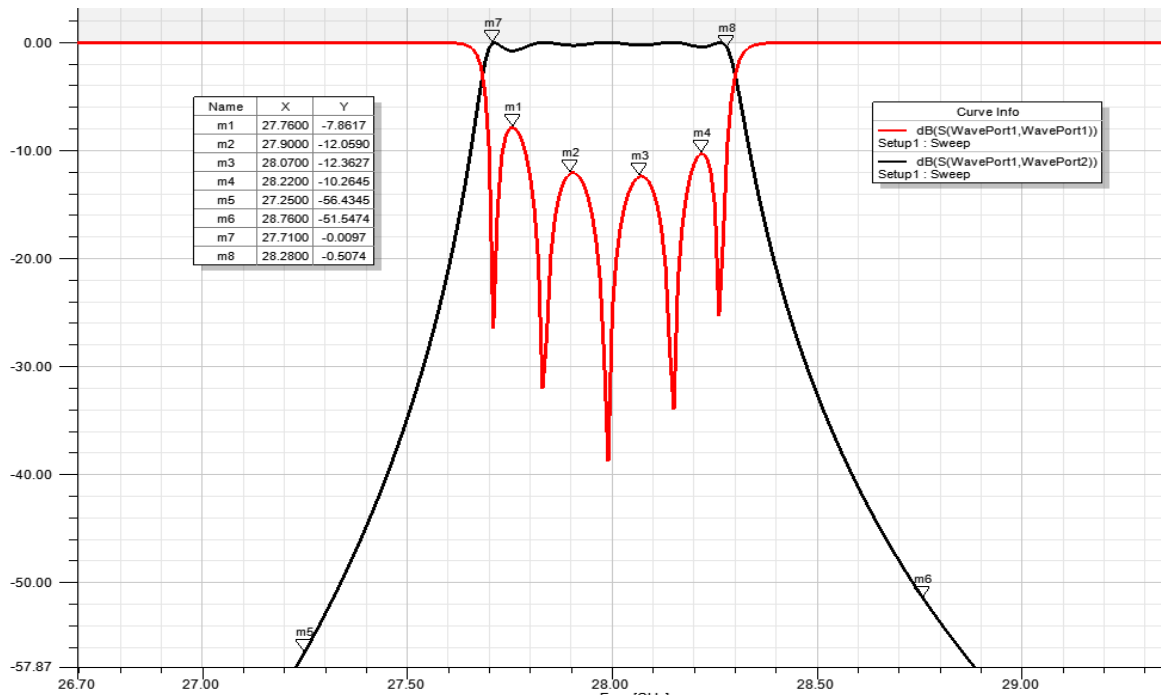*Figure 4. 20: The S-parameters simulation results*

4.3 Chapter Summary

This chapter starts with the theoretical principles for designing the iris waveguide bandpass filter. The mathematical model for the waveguide filter is first derived. Next, the detailed steps involved in constructing an HFSS simulation model are described. Finally, the S-parameters simulation results are analyzed and discussed.

CHAPTER 5

CONCLUSION AND RECOMMENDATIONS

This dissertation presents the design of a WR-34 band millimeter-wave iris waveguide bandpass filter. The filter operates at 28 GHz center frequency. A working simulation model by using the HFSS simulation software is also presented. The main contribution of the designed filter in this dissertation is that it serves as a vital component to discriminate between the desired and undesired frequency signals for future 5G communication networks. The 5G technology uses millimeter-wave as its backbone because millimeter-wave is still under-utilized and is able to provide a large bandwidth and a fast data transfer rate. This technology is needed because network congestion is expected to occur owing to the demand capacity of the spectrum based services.

The mathematical model and the corresponding simulation model in HFSS have been presented in detail in Chapters 3 and 4. In this research, the mathematical model of the waveguide bandpass filter is first derived based on Maxwell's equation and the basic waveguide theorem. An insertion loss method with a Chebyshev polynomial is used to synthesize the desired filter response. A mathematical package, i.e., Maple, is used as a support tool for deriving the mathematical model. The mathematical model is then validated by constructing a working simulation model using the HFSS simulation software. The S-parameter simulation results depict that the center frequency of the filter is at 27.995 GHz. The lower stopband frequency (fp1) is 27.71 GHz while the upper stopband frequency (fp2) is 28.28 GHz. Therefore, the passband ranges from 27.71 GHz to 28.28 GHz with a relative bandwidth of 2.03%. The return loss for the entire passband

is better than 7.8 dB. The S-parameter simulation results also indicate that the filter has an upper and lower stopband insertion loss measurements of better than 40 dB at 27.25 GHz and 28.75 GHz respectively. This filter can achieve a 570 MHz bandwidth with S11 ≤ -7.8 dB and S21 ≤ 1dB.

Owing to the lack of facilities to fabricate the proposed bandpass filter design, the target of this project is confined to mathematical formulation of the designed filter and its validation with a working simulation model. For further work, it is highly recommended to fabricate the mm-wave waveguide bandpass filter. The main purpose is to compare the actual filter performance with the simulation results.

REFERENCES

[1]   F. Khan, Z. Pi, and S. Rajagopal, "Millimeter-wave mobile broadband with large scale spatial processing for 5G mobile communication," in *2012 50th Annual Allerton Conference on Communication, Control, and Computing (Allerton)*, 2012, pp. 1517-1523.

[2]   Z. Pi and F. Khan, "An introduction to millimeter-wave mobile broadband systems," *IEEE Communications Magazine,* vol. 49, pp. 101-107, 2011.

[3]   White_paper_c11-481360, "Cisco Visual Networking Index: Forecast and Methodology," June 2010.

[4]   S. K. Agrawal and K. Sharma, "5G millimeter wave (mmWave) communications," in *2016 3rd International Conference on Computing for Sustainable Global Development (INDIACom)*, 2016, pp. 3630-3634.

[5]   M. M. Ahamed and S. Faruque, "Propagation factors affecting the performance of 5G millimeter wave radio channel," in *2016 IEEE International Conference on Electro Information Technology (EIT)*, 2016, pp. 0728-0733.

[6]   R. Ford, M. Zhang, M. Mezzavilla, S. Dutta, S. Rangan, and M. Zorzi, "Achieving Ultra-Low Latency in 5G Millimeter Wave Cellular Networks," *IEEE Communications Magazine,* vol. 55, pp. 196-203, 2017.

[7]   J. Qiao, X. S. Shen, J. W. Mark, Q. Shen, Y. He, and L. Lei, "Enabling device-to-device communications in millimeter-wave 5G cellular networks," *IEEE Communications Magazine,* vol. 53, pp. 209-215, 2015.

[8]   T. S. Rappaport, S. Sun, R. Mayzus, H. Zhao, Y. Azar, K. Wang, *et al.*, "Millimeter Wave Mobile Communications for 5G Cellular: It Will Work!," *IEEE Access,* vol. 1, pp. 335-349, 2013.

[9]   F. Saadaoui, M. Fathallah, A. Ragheb, I. Memon, H. Fathallah, and S. Alshebeili, "Optimizing OSSB Generation Using Semiconductor Optical Amplifier (SOA) for 5G Millimeter Wave Switching," *IEEE Access,* vol. PP, pp. 1-1, 2017.

[10]   J. Zhang, X. Ge, Q. Li, M. Guizani, and Y. Zhang, "5G Millimeter-Wave Antenna Array: Design and Challenges," *IEEE Wireless Communications,* vol. PP, pp. 2-8, 2017.

[11]   G. R. MacCartney, Z. Junhong, N. Shuai, and T. S. Rappaport, "Path loss models for 5G millimeter wave propagation channels in urban microcells," in *2013 IEEE Global Communications Conference (GLOBECOM)*, 2013, pp. 3948-3953.

[12]   Y. Tao, B. Zhang, D. Fang, and Y. Fan, "An 110GHz waveguide bandpass filter using iris inductive window coupled structure," in *2016 IEEE 9th UK-Europe-China Workshop on Millimetre Waves and Terahertz Technologies (UCMMT)*, 2016, pp. 227-228.

[13]   T. Zou, B. Zhang, and Y. Fan, "Design of a 73GHz waveguide bandpass filter," in *2016 IEEE 9th UK-Europe-China Workshop on Millimetre Waves and Terahertz Technologies (UCMMT)*, 2016, pp. 219-221.

[14]   D. Fang, B. Zhang, and J. He, "A E-band E-plane type waveguide bandpass filter," in *2016 IEEE 9th UK-Europe-China Workshop on Millimetre Waves and Terahertz Technologies (UCMMT)*, 2016, pp. 180-182.

[15]   J. Wang, Y. Li, and J. Wang, "Millimeter-wave horizontally polarized end-fire magneto-electric dipole antenna array," in *2016 IEEE 9th UK-Europe-China Workshop on Millimetre Waves and Terahertz Technologies (UCMMT)*, 2016, pp. 12-14.

[16]   M. K. B. Zahari, "Design & Development of Rectangular Waveguide Bandpass Filter," Bachelor of Electronic (Computer Engineering) with Honours, Faculty of Electronic and Computer Engineering, Universiti Teknikal Malaysia Melaka, 2010.

[17]   I. Hunter, "Theory and Design of Microwave Filters ", ed London, United Kingdom: The Institution of Engineering and Technology, 2001, pp. 200-266.

[18]   J. Jian-Ming, "Basic Electromagnetic Theory," in *Theory and Computation of Electromagnetic Fields*, ed: Wiley-IEEE Press, 2010, pp. 1-42.

[19]   E. C. Robert, "Basic Electromagnetic Theory," in *Field Theory of Guided Waves*, ed: Wiley-IEEE Press, 1991, pp. 1-54.

[20]   F. P. Andrew, L. R. Scott, and M. Raj, "Electromagnetic Theory," in *Computational Methods for Electromagnetics*, ed: Wiley-IEEE Press, 1998, pp. 1-36.

[21] E. C. Robert, "Electromagnetic Theory," in *Foundations for Microwave Engineering*, ed: Wiley-IEEE Press, 2001, pp. 17-70.

[22] S. Levent, "Electromagnetic Theory: Basic Review," in *Electromagnetic Modeling and Simulation*, ed: Wiley-IEEE Press, 2014, p. 696.

[23] F. T. Ulaby, "Fundamental of Applied Electromagnetics ", ed Upper Saddle River Pearson - Prentice Hall, 1994, pp. 320-371.

[24] Signus. (2013). *Transverse Magnetic (TM) and Transverse Electric (TE) modes*. Available: http://physics.stackexchange.com/questions/78419/transverse-magnetic-tm-and-transverse-electric-te-modes

[25] M. Marcus and B. Pattan, "Millimeter wave propagation; spectrum management implications," *IEEE Microwave Magazine,* vol. 6, pp. 54-62, 2005.

[26] Y. Azar, G. N. Wong, K. Wang, R. Mayzus, J. K. Schulz, H. Zhao*, et al.*, "28 GHz propagation measurements for outdoor cellular communications using steerable beam antennas in New York city," in *2013 IEEE International Conference on Communications (ICC)*, 2013, pp. 5143-5147.

[27] A. I. Sulyman, A. Alwarafy, G. R. MacCartney, T. S. Rappaport, and A. Alsanie, "Directional Radio Propagation Path Loss Models for Millimeter-Wave Wireless Networks in the 28-, 60-, and 73-GHz Bands," *IEEE Transactions on Wireless Communications,* vol. 15, pp. 6939-6947, 2016.

[28] H. A. Wheeler, "Formulas for the Skin Effect," *Proceedings of the IRE,* vol. 30, pp. 412-424, 1942.

[29] K. Blattenberger. (2008). *Skin Depth (aka Skin Effect) as a Function of Frequency, Permeability, &Conductivity*. Available: http://www.rfcafe.com/references/electrical/skin-depth.htm

[30] M. Kostylev. (2006). *Skin Depth* Available: https://www.microwaves101.com/encyclopedias/skin-depth

[31] n/a. (2009). *Electrical Losses due to Skin Effect and Proximity Effect*. Available: http://ep2000.com/uploads/EP_WhitePaper_SkinEffect.pdf

[32] P. Vateekul. (2004). *Why waveguide has a very low loss due to skin effect* Available: http://armymunitions.tpub.com/mm50058/mm500580176.htm

[33] I. Poole. (n.d.). *WG and WR waveguide dimensions and sizes*. Available: http://www.radio-electronics.com/info/antennas/waveguide/rf-waveguide-dimensions-sizes.php

[34] G.Matthaei, L.Young, and E.M.T.Jones, *MICROWAVES FILTERS, IMPEDANCE-MATCHING NETWORKS, AND COUPLING STRUCTURES*. Boston,London: Artech House Publishers, 1980.

APPENDICES

APPENDIX A

Mathematical Modelling of the 28GHz Millimeter-wave Waveguide Bandpass Filter

In this project, the millimeter-wave waveguide bandpass filter design specifications are as follows:

Passband   27.70GHz - 28.30GHz
Passband Return Loss   ≥ 20dB
Stopband Inserion Loss   ≥ 40dB at 27.25GHz
                            ≥ 40dB at 28.75GHz

A suitable rectangular waveguide to meet the specifications is WR-34 band waveguide. The lowest order mode, TE10 cut-off frequency for WR -34 is 17.357 GHz and the dimensions is 0.340 inches x 0.170 inches.

Therefore,

$f1 := 27.70 \cdot 10^9$

$$2.770000000 \ 10^{10} \tag{1}$$

$f2 := 28.30 \cdot 10^9$

$$2.830000000 \ 10^{10} \tag{2}$$

$fs1 := 27.25 \cdot 10^9$

$$2.725000000 \ 10^{10} \tag{3}$$

$fs2 := 28.75 \cdot 10^9$

$$2.875000000 \ 10^{10} \tag{4}$$

$LA1 := 40$

$$40 \tag{5}$$

$LA2 := 40$

$$40 \tag{6}$$

$LR := 20$

$$20 \tag{7}$$

$fc := 17.357 \cdot 10^9$

$$1.735700000 \ 10^{10} \tag{8}$$

$c := 3.0 \cdot 10^8$

$$3.000000000 \ 10^8 \tag{9}$$

The ripple level of the waveguide bandpass filter is determined, as follows

$$\varepsilon := \left(\cfrac{1}{1 - 10^{-\frac{LR}{10}}} - 1 \right)^{\frac{1}{2}};$$

$$\frac{1}{99}\sqrt{99} \tag{10}$$

By applying the formula c=fλ yields,

$$\lambda 1 := \frac{c}{f1};$$

$$0.01083032491 \tag{11}$$

$$\lambda 2 := \frac{c}{f2};$$

$$0.01060070671 \tag{12}$$

The guide wavelength, λg1 and λg2 are then determined, as follows:

$$\lambda g1 := \cfrac{\lambda 1}{\left(1 - \left(\cfrac{2.\,\pi.fc}{2.\,\pi.f1} \right)^{2} \right)^{\frac{1}{2}}};$$

$$0.01389686557 \tag{13}$$

$$\lambda g2 := \cfrac{\lambda 2}{\left(1 - \left(\cfrac{2.\,\pi.fc}{2.\,\pi.f2} \right)^{2} \right)^{\frac{1}{2}}};$$

$$0.01342144788 \tag{14}$$

Let the guide wavelength when the guide is half wavelength long be λg0, hence λg0 can be calculated as follows:

$$\lambda g0 := \frac{\lambda g1 + \lambda g2}{2} + \frac{1}{\pi} \left(\cfrac{\lambda g1 \cdot \cos\left(\frac{\pi}{2} \cdot \frac{\lambda g2}{\lambda g1} \right) + \lambda g2 \cdot \cos\left(\frac{\pi}{2} \cdot \frac{\lambda g1}{\lambda g2} \right)}{\sin\left(\frac{\pi}{2} \cdot \frac{\lambda g2}{\lambda g1} \right) + \sin\left(\frac{\pi}{2} \cdot \frac{\lambda g1}{\lambda g2} \right)} \right);$$

$$0.01365916085 \tag{15}$$

The attentuation constant, α is calculated as follows:

$$\alpha := \left(\frac{\lambda g I}{\lambda g 0} \cdot \sin\left(\frac{\pi \cdot \lambda g 0}{\lambda g I} \right) \right)^{-1} ;$$

$$18.29975928 \qquad\qquad (16)$$

The next steps is to determine the required filter order, N. The filter order can be determined by analyzing the following insertion lose function subject to different numbers of N, where T_n is the Chebyshev Polynomials.

$$L = 10\log_{10}\left(1 + \varepsilon^2 T_n^{\ 2}\left(\frac{\alpha \lambda g}{\lambda g 0} \sin\left(\frac{\pi \lambda g 0}{\lambda g} \right) \right) \right)$$

$$\lambda g := \frac{c}{f \cdot \sqrt{1 - \left(\frac{fc}{f} \right)^2}} ;$$

$$\frac{3.000000000 \ 10^8}{f \sqrt{1 - \dfrac{3.012654490 \ 10^{20}}{f^2}}} \qquad\qquad (17)$$

$$k := \frac{\alpha \cdot \lambda g}{\lambda g 0} \cdot \sin\left(\pi \cdot \frac{\lambda g 0}{\lambda g} \right) ;$$

$$\frac{4.019227714 \ 10^{11} \sin\left(1.430383980 \ 10^{-10} f \sqrt{1 - \dfrac{3.012654490 \ 10^{20}}{f^2}} \right)}{f \sqrt{1 - \dfrac{3.012654490 \ 10^{20}}{f^2}}} \qquad\qquad (18)$$

$$x := k;$$

$$\frac{4.019227714 \ 10^{11} \sin\left(1.430383980 \ 10^{-10} f \sqrt{1 - \dfrac{3.012654490 \ 10^{20}}{f^2}} \right)}{f \sqrt{1 - \dfrac{3.012654490 \ 10^{20}}{f^2}}} \qquad\qquad (19)$$
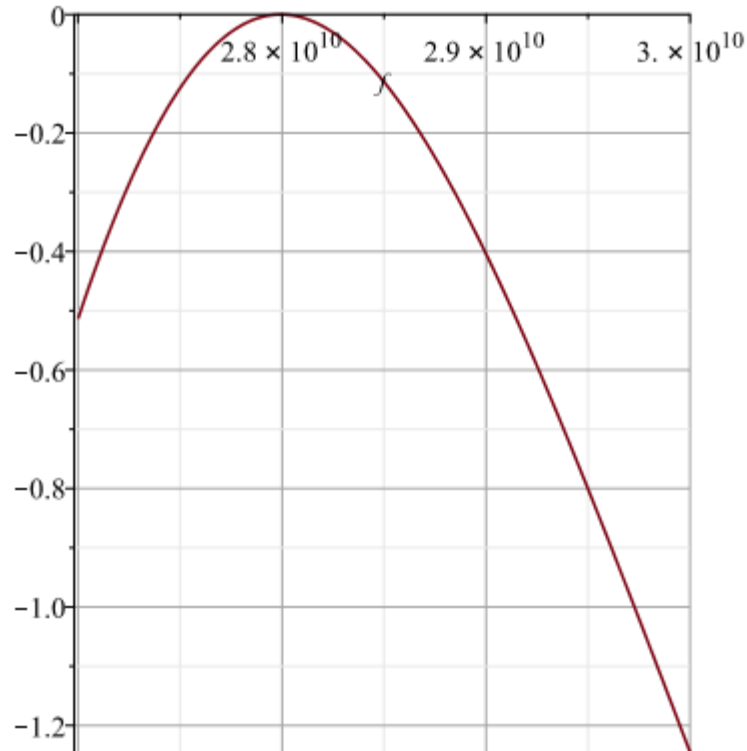
When N=1,

$$T1 := x;$$

$$\frac{4.019227714 \cdot 10^{11} \sin\left(1.430383980 \cdot 10^{-10} f \sqrt{1 - \frac{3.012654490 \cdot 10^{20}}{f^2}}\right)}{f \sqrt{1 - \frac{3.012654490 \cdot 10^{20}}{f^2}}} \tag{20}$$

$$S211 := 10 \cdot \log_{10}\left(\frac{1}{\left(1 + (0.1)^2 \cdot \text{abs}(T1)^2\right)}\right);$$

$$-\frac{10 \ln\left(1 + 1.615419142 \cdot 10^{21} \left|\frac{\sin\left(1.430383980 \cdot 10^{-10} f \sqrt{1 - \frac{3.012654490 \cdot 10^{20}}{f^2}}\right)}{f \sqrt{1 - \frac{3.012654490 \cdot 10^{20}}{f^2}}}\right|^2\right)}{\ln(10)} \tag{21}$$

$plot\left(S211, f = 27 \cdot 10^9 .. 30 \cdot 10^9, gridlines\right)$

When N=2,

$T2 := 2\,x^2 - 1;$

$$\frac{3.230838284\ 10^{23} \sin\left(1.430383980\ 10^{-10} f\ \sqrt{1 - \dfrac{3.012654490\ 10^{20}}{f^2}}\right)^2}{f^2\left(1 - \dfrac{3.012654490\ 10^{20}}{f^2}\right)} - 1 \qquad (22)$$

$S212 := 10 \cdot \log_{10}\left(\dfrac{1}{(1 + (0.1)^2.\ \mathrm{abs}(T2)^2)}\right);$

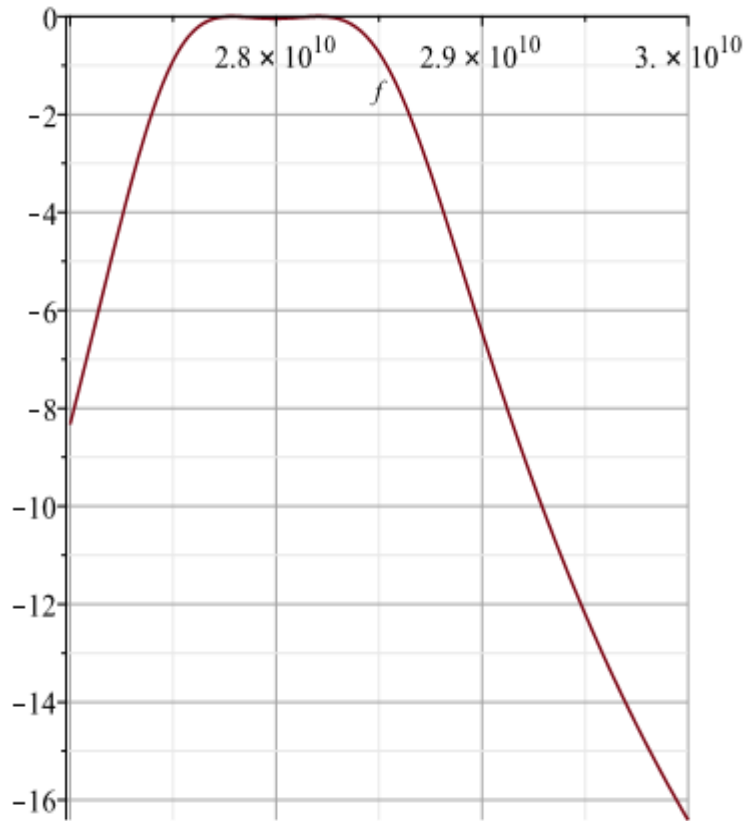$$-\frac{1}{\ln(10)}\left(10 \ln\left(1\right.\right. \qquad (23)$$

$$\left.\left. + 0.01\left|\frac{3.230838284\ 10^{23} \sin\left(1.430383980\ 10^{-10} f\ \sqrt{1 - \dfrac{3.012654490\ 10^{20}}{f^2}}\right)^2}{f^2\left(1 - \dfrac{3.012654490\ 10^{20}}{f^2}\right)} - 1\right|^2\right)\right)$$

$plot(S212, f = 27 \cdot 10^9 .. 30 \cdot 10^9, gridlines)$

When N=3;

$T3 := 4 \cdot x^3 - 3 \cdot x;$

$$\frac{2.597094954 \ 10^{35} \sin\left(1.430383980 \ 10^{-10} f \ \sqrt{1 - \frac{3.012654490 \ 10^{20}}{f^2}}\right)^3}{f^3 \left(1 - \frac{3.012654490 \ 10^{20}}{f^2}\right)^{3/2}} \tag{24}$$
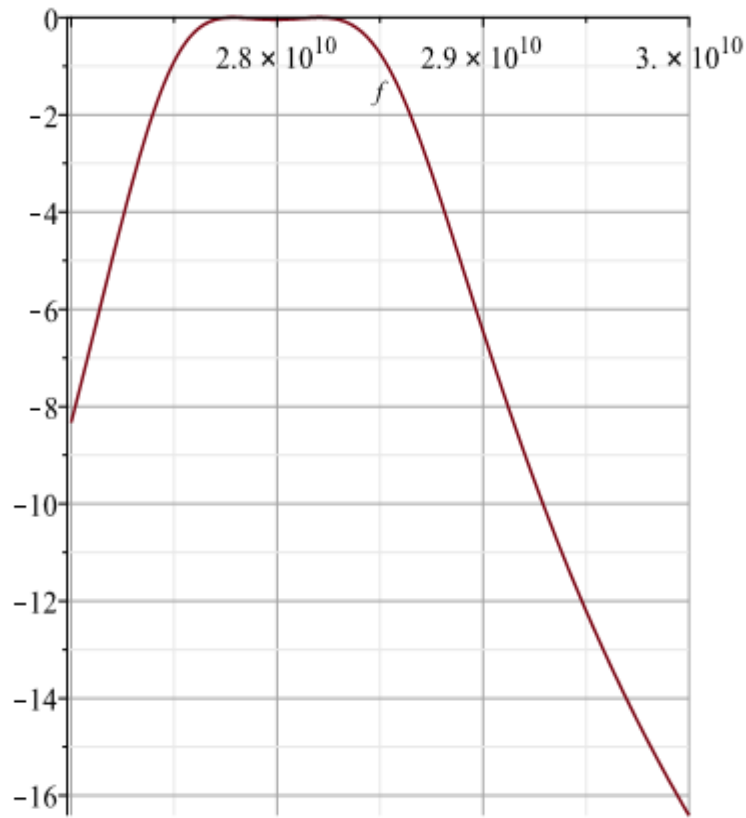
$$- \frac{1.205768314 \ 10^{12} \sin\left(1.430383980 \ 10^{-10} f \ \sqrt{1 - \frac{3.012654490 \ 10^{20}}{f^2}}\right)}{f \ \sqrt{1 - \frac{3.012654490 \ 10^{20}}{f^2}}}$$

$S213 := 10 \cdot \log_{10}\left(\frac{1}{(1 + (0.1)^2 \cdot abs(T3)^2)}\right);$

62

$$-\frac{1}{\ln(10)}\left(\ \left|\ 10\ln\left(\ 1+0.01\ \left|\ \right.\right.\right.\right.$$

(25)

$$-\frac{2.597094954\ 10^{35}\sin\left(1.430383980\ 10^{-10}f\ \sqrt{1-\dfrac{3.012654490\ 10^{20}}{f^2}}\ \right)^3}{f^3\left(1-\dfrac{3.012654490\ 10^{20}}{f^2}\right)^{3/2}}$$

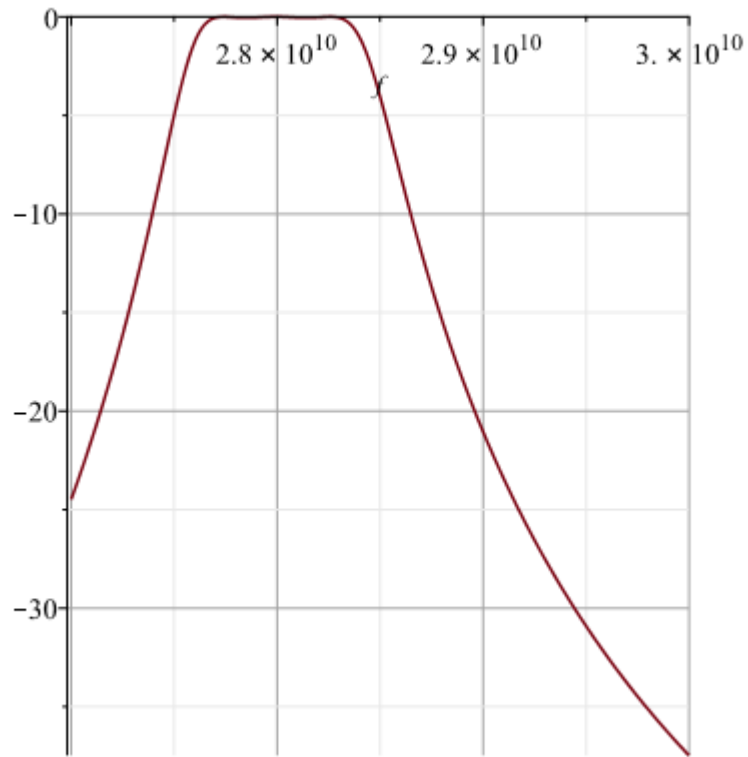$$+\frac{1.205768314\ 10^{12}\sin\left(1.430383980\ 10^{-10}f\ \sqrt{1-\dfrac{3.012654490\ 10^{20}}{f^2}}\ \right)}{f\ \sqrt{1-\dfrac{3.012654490\ 10^{20}}{f^2}}}\ \left|\ \right.^2\left.\right)\right)$$

$$plot\left(S213, f=27\cdot10^9\,..30\cdot10^9, gridlines\right)$$
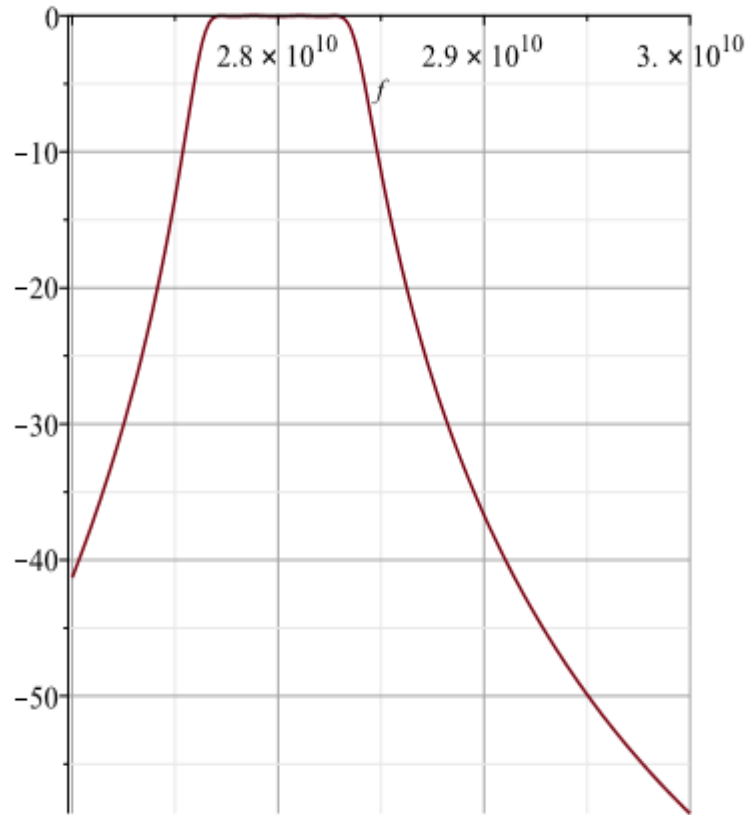
When N=4,

$T4 := 8 \cdot x^4 - 8 \cdot x^2 + 1;$

$$\frac{2.087663202\ 10^{47} \sin\left(1.430383980\ 10^{-10} f \sqrt{1 - \dfrac{3.012654490\ 10^{20}}{f^2}}\right)^4}{f^4 \left(1 - \dfrac{3.012654490\ 10^{20}}{f^2}\right)^2}$$

$$- \frac{1.292335314\ 10^{24} \sin\left(1.430383980\ 10^{-10} f \sqrt{1 - \dfrac{3.012654490\ 10^{20}}{f^2}}\right)^2}{f^2 \left(1 - \dfrac{3.012654490\ 10^{20}}{f^2}\right)} + 1$$

(26)

$S214 := 10 \cdot \log_{10}\left(\dfrac{1}{(1 + (0.1)^2 \cdot \text{abs}(T4)^2)}\right);$

$$-\frac{1}{\ln(10)}\left(10 \ln\left(1 \right.\right.$$

$$+ 0.01 \left| \frac{2.087663202\ 10^{47} \sin\left(1.430383980\ 10^{-10} f \sqrt{1 - \dfrac{3.012654490\ 10^{20}}{f^2}}\right)^4}{f^4 \left(1 - \dfrac{3.012654490\ 10^{20}}{f^2}\right)^2}\right.$$

$$\left.\left.\left.- \frac{1.292335314\ 10^{24} \sin\left(1.430383980\ 10^{-10} f \sqrt{1 - \dfrac{3.012654490\ 10^{20}}{f^2}}\right)^2}{f^2 \left(1 - \dfrac{3.012654490\ 10^{20}}{f^2}\right)} + 1 \right|^2\right)\right)$$

(27)

$$-\frac{1}{\ln(10)}\left(10 \ln\left(1 \right.\right.$$

$$+ 0.01 \left| \frac{5.973147226\ 10^{41} \sin\left(5.195858140\ 10^{-10} f \sqrt{1 - \dfrac{4.303360000\ 10^{19}}{f^2}}\right)^4}{f^4 \left(1 - \dfrac{4.303360000\ 10^{19}}{f^2}\right)^2}\right.$$

$$\left.\left.\left.- \frac{2.185982109\ 10^{21} \sin\left(5.195858140\ 10^{-10} f \sqrt{1 - \dfrac{4.303360000\ 10^{19}}{f^2}}\right)^2}{f^2 \left(1 - \dfrac{4.303360000\ 10^{19}}{f^2}\right)} + 1 \right|^2\right)\right)$$

(28)

$plot(S214, f = 27 \cdot 10^9 .. 30 \cdot 10^9, gridlines)$

When N=5,

$$T5 := 16 \cdot x^5 - 20 \cdot x^3 + 5 \cdot x;$$

$$\frac{1.678158760 \ 10^{59} \sin\left(1.430383980 \ 10^{-10} f \sqrt{1 - \dfrac{3.012654490 \ 10^{20}}{f^2}}\right)^5}{f^5 \left(1 - \dfrac{3.012654490 \ 10^{20}}{f^2}\right)^{5/2}} \tag{29}$$

$$- \frac{1.298547477 \ 10^{36} \sin\left(1.430383980 \ 10^{-10} f \sqrt{1 - \dfrac{3.012654490 \ 10^{20}}{f^2}}\right)^3}{f^3 \left(1 - \dfrac{3.012654490 \ 10^{20}}{f^2}\right)^{3/2}}$$

65

$$+ \frac{2.009613857 \ 10^{12} \sin\left(1.430383980 \ 10^{-10} f \sqrt{1 - \dfrac{3.012654490 \ 10^{20}}{f^2}} \right)}{f \sqrt{1 - \dfrac{3.012654490 \ 10^{20}}{f^2}}}$$

$$\frac{1.974747275 \ 10^{52} \sin\left(5.195858140 \ 10^{-10} f \sqrt{1 - \dfrac{4.303360000 \ 10^{19}}{f^2}} \right)^5}{f^5 \left(1 - \dfrac{4.303360000 \ 10^{19}}{f^2} \right)^{5/2}} \qquad \textbf{(30)}$$

$$- \frac{9.033684524 \ 10^{31} \sin\left(5.195858140 \ 10^{-10} f \sqrt{1 - \dfrac{4.303360000 \ 10^{19}}{f^2}} \right)^3}{f^3 \left(1 - \dfrac{4.303360000 \ 10^{19}}{f^2} \right)^{3/2}}$$

$$+ \frac{8.265103805 \ 10^{10} \sin\left(5.195858140 \ 10^{-10} f \sqrt{1 - \dfrac{4.303360000 \ 10^{19}}{f^2}} \right)}{f \sqrt{1 - \dfrac{4.303360000 \ 10^{19}}{f^2}}}$$

$$S215 := 10 \cdot \log_{10}\left(\frac{1}{\left(1 + (0.1)^2 \cdot \text{abs}(T5)^2 \right)} \right);$$

$$-\frac{1}{\ln(10)} \left(10 \ln\left(1 \vphantom{\frac{1}{1}} \right. \right. \qquad \textbf{(31)}$$

$$\left. \left. + 0.01 \left| \frac{1.678158760 \ 10^{59} \sin\left(1.430383980 \ 10^{-10} f \sqrt{1 - \dfrac{3.012654490 \ 10^{20}}{f^2}} \right)^5}{f^5 \left(1 - \dfrac{3.012654490 \ 10^{20}}{f^2} \right)^{5/2}} \right. \right. \right.$$
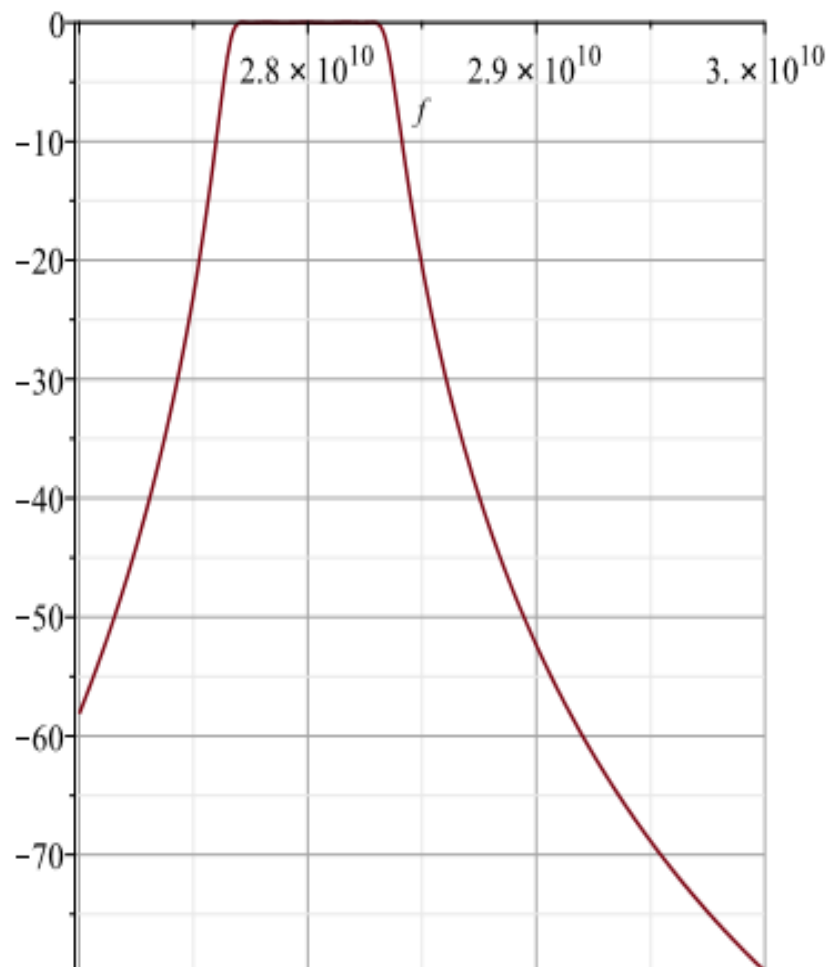
66

$$-\frac{1.298547477\ 10^{36}\sin\left(1.430383980\ 10^{-10}f\sqrt{1-\dfrac{3.012654490\ 10^{20}}{f^2}}\right)^3}{f^3\left(1-\dfrac{3.012654490\ 10^{20}}{f^2}\right)^{3/2}}$$

$$+\frac{2.009613857\ 10^{12}\sin\left(1.430383980\ 10^{-10}f\sqrt{1-\dfrac{3.012654490\ 10^{20}}{f^2}}\right)}{f\sqrt{1-\dfrac{3.012654490\ 10^{20}}{f^2}}}\Bigg)\Bigg)^2\Bigg)\Bigg)$$

$plot\left(S215, f=27\cdot10^9..30\cdot10^9, gridlines\right)$

When N=5, the response meet the filter specifications, i.e., satisfying the most severe specifications on the insertion loss. Therefore, the required filter order is

$N := 5;$

$$5 \qquad\qquad (32)$$

Next, we proceed to calculate the characteristics impedance of free space, n.

$$n := \sinh\left(\frac{1}{N}\sinh^{-1}\left(\frac{1}{0.1}\right)\right);$$

$$0.6362322962 \qquad\qquad (33)$$

The protptype element values (normalised to 1 ohm) are then determined, as follows:

$r := 0;$

$$0 \qquad\qquad (34)$$

$Z0 := 1;$

$$1 \qquad\qquad (35)$$

$r := 1;$

$$1 \qquad\qquad (36)$$

$$Z1 := evalf\left(\frac{2 \cdot \alpha}{n} \cdot \sin\left(\frac{(2 \cdot r - 1) \cdot \pi}{2 \cdot N}\right) - \frac{1}{4 \cdot n \cdot \alpha}\left(\frac{n^2 + \sin^2\left(\frac{r \cdot \pi}{N}\right)}{\sin\left(\frac{(2 \cdot r + 1) \cdot \pi}{2 \cdot N}\right)}\right.\right.$$
$$\left.\left. + \frac{n^2 + \sin^2\left(\frac{(r-1) \cdot \pi}{N}\right)}{\sin\left(\frac{(2 \cdot r - 3) \cdot \pi}{2 \cdot N}\right)}\right)\right);$$

$$17.78454066 \qquad\qquad (37)$$

$r := 2;$

$$2 \qquad\qquad (38)$$

$$Z2 := evalf\left(\frac{2 \cdot \alpha}{n} \cdot \sin\left(\frac{(2 \cdot r - 1) \cdot \pi}{2 \cdot N} \right) - \frac{1}{4 \cdot n \cdot \alpha} \left(\frac{n^2 + \sin^2\left(\frac{r \cdot \pi}{N} \right)}{\sin\left(\frac{(2 \cdot r + 1) \cdot \pi}{2 \cdot N} \right)} \right. \right.$$
$$\left. \left. + \frac{n^2 + \sin^2\left(\frac{(r-1) \cdot \pi}{N} \right)}{\sin\left(\frac{(2 \cdot r - 3) \cdot \pi}{2 \cdot N} \right)} \right) \right);$$

$$46.45878000 \tag{39}$$

$r := 3;$

$$3 \tag{40}$$

$$Z3 := evalf\left(\frac{2 \cdot \alpha}{n} \cdot \sin\left(\frac{(2 \cdot r - 1) \cdot \pi}{2 \cdot N} \right) - \frac{1}{4 \cdot n \cdot \alpha} \left(\frac{n^2 + \sin^2\left(\frac{r \cdot \pi}{N} \right)}{\sin\left(\frac{(2 \cdot r + 1) \cdot \pi}{2 \cdot N} \right)} \right. \right.$$
$$\left. \left. + \frac{n^2 + \sin^2\left(\frac{(r-1) \cdot \pi}{N} \right)}{\sin\left(\frac{(2 \cdot r - 3) \cdot \pi}{2 \cdot N} \right)} \right) \right);$$

$$57.45590104 \tag{41}$$

$r := 4;$

$$4 \tag{42}$$

$$Z4 := evalf\left(\frac{2 \cdot \alpha}{n} \cdot \sin\left(\frac{(2 \cdot r - 1) \cdot \pi}{2 \cdot N} \right) - \frac{1}{4 \cdot n \cdot \alpha} \left(\frac{n^2 + \sin^2\left(\frac{r \cdot \pi}{N} \right)}{\sin\left(\frac{(2 \cdot r + 1) \cdot \pi}{2 \cdot N} \right)} \right. \right.$$
$$\left. \left. + \frac{n^2 + \sin^2\left(\frac{(r-1) \cdot \pi}{N} \right)}{\sin\left(\frac{(2 \cdot r - 3) \cdot \pi}{2 \cdot N} \right)} \right) \right);$$

$$46.45878000 \tag{43}$$

$r := 5;$

$$5 \tag{44}$$

$$Z5 := evalf\left(\frac{2 \cdot \alpha}{n} \cdot \sin\left(\frac{(2 \cdot r - 1) \cdot \pi}{2 \cdot N} \right) - \frac{1}{4 \cdot n \cdot \alpha} \left(\frac{n^2 + \sin^2\left(\frac{r \cdot \pi}{N} \right)}{\sin\left(\frac{(2 \cdot r + 1) \cdot \pi}{2 \cdot N} \right)} \right. \right.$$
$$\left. \left. + \frac{n^2 + \sin^2\left(\frac{(r-1) \cdot \pi}{N} \right)}{\sin\left(\frac{(2 \cdot r - 3) \cdot \pi}{2 \cdot N} \right)} \right) \right);$$

$$17.78454066 \tag{45}$$

$r := 6;$

$$6 \tag{46}$$

$Z6 := 1;$

$$1 \tag{47}$$

$r := 0;$

$$0 \tag{48}$$

$$K01 := evalf\left(\frac{\left(n^2 + \sin^2\left(\frac{r \cdot \pi}{N} \right) \right)^{\frac{1}{2}}}{n} \right);$$

$$1.000000000 \tag{49}$$

$r := 1;$

$$1 \tag{50}$$

$$K12 := evalf\left(\frac{\left(n^2 + \sin^2\left(\frac{r \cdot \pi}{N} \right) \right)^{\frac{1}{2}}}{n} \right);$$

$$1.361434818 \tag{51}$$

$r := 2;$

$$2 \tag{52}$$

$$K23 := evalf\left(\frac{\left(n^2 + \sin^2\left(\frac{r \cdot \pi}{N} \right) \right)^{\frac{1}{2}}}{n} \right);$$

$$1.798472818 \tag{53}$$

$r := 3;$

$$3 \tag{54}$$

$$K34 := evalf\left(\frac{\left(n^2 + \sin^2\left(\frac{r \cdot \pi}{N}\right)\right)^{\frac{1}{2}}}{n}\right);$$

$$1.798472818 \tag{55}$$

$$r := 4;$$

$$4 \tag{56}$$

$$K45 := evalf\left(\frac{\left(n^2 + \sin^2\left(\frac{r \cdot \pi}{N}\right)\right)^{\frac{1}{2}}}{n}\right);$$

$$1.361434818 \tag{57}$$

$$r := 5;$$

$$5 \tag{58}$$

$$K56 := evalf\left(\frac{\left(n^2 + \sin^2\left(\frac{r \cdot \pi}{N}\right)\right)^{\frac{1}{2}}}{n}\right);$$

$$1.000000000 \tag{59}$$

The next steps is to determine the susceptances of the inductive irises,

$$r := 0;$$

$$0 \tag{60}$$

$$B01 := evalf\left(\frac{(Z0 \cdot Z1)^{\frac{1}{2}}}{K01} - \frac{K01}{(Z0 \cdot Z1)^{\frac{1}{2}}}\right);$$

$$3.980046390 \tag{61}$$

$$r := 1;$$

$$1 \tag{62}$$

$$B12 := evalf\left(\frac{(Z1 \cdot Z2)^{\frac{1}{2}}}{K12} - \frac{K12}{(Z1 \cdot Z2)^{\frac{1}{2}}}\right);$$

$$21.06604636 \tag{63}$$

$r := 2;$
$$2 \tag{64}$$

$$B23 := evalf\left(\frac{(Z2 \cdot Z3)^{\frac{1}{2}}}{K23} - \frac{K23}{(Z2 \cdot Z3)^{\frac{1}{2}}} \right);$$

$$28.69265762 \tag{65}$$

$r := 3;$
$$3 \tag{66}$$

$$B34 := evalf\left(\frac{(Z3 \cdot Z4)^{\frac{1}{2}}}{K34} - \frac{K34}{(Z3 \cdot Z4)^{\frac{1}{2}}} \right);$$

$$28.69265762 \tag{67}$$

$r := 4;$
$$4 \tag{68}$$

$$B45 := evalf\left(\frac{(Z4 \cdot Z5)^{\frac{1}{2}}}{K45} - \frac{K45}{(Z4 \cdot Z5)^{\frac{1}{2}}} \right);$$

$$21.06604636 \tag{69}$$

$r := 5;$
$$5 \tag{70}$$

$$B56 := evalf\left(\frac{(Z5 \cdot Z6)^{\frac{1}{2}}}{K56} - \frac{K56}{(Z5 \cdot Z6)^{\frac{1}{2}}} \right);$$

$$3.980046390 \tag{71}$$

Next, the phase of the guide between the irises are determined:

$r := 1;$
$$1 \tag{72}$$

$$\psi 1 := \pi - \frac{1}{2} \left(\cot^{-1}\left(\frac{B12}{2} \right) + \cot^{-1}\left(\frac{B01}{2} \right) \right);$$

$$2.861439277 \tag{73}$$

$$r := 2;$$

$$2 \tag{74}$$

$$\psi 2 := \pi - \frac{1}{2} \left(\cot^{-1}\left(\frac{B23}{2} \right) + \cot^{-1}\left(\frac{B12}{2} \right) \right);$$

$$3.059468918 \tag{75}$$

$$r := 3;$$

$$3 \tag{76}$$

$$\psi 3 := \pi - \frac{1}{2} \left(\cot^{-1}\left(\frac{B34}{2} \right) + \cot^{-1}\left(\frac{B23}{2} \right) \right);$$

$$3.072000973 \tag{77}$$

$$r := 4;$$

$$4 \tag{78}$$

$$\psi 4 := \pi - \frac{1}{2} \left(\cot^{-1}\left(\frac{B45}{2} \right) + \cot^{-1}\left(\frac{B34}{2} \right) \right);$$

$$3.059468918 \tag{79}$$

$$r := 5;$$

$$5 \tag{80}$$

$$\psi 5 := \pi - \frac{1}{2} \left(\cot^{-1}\left(\frac{B56}{2} \right) + \cot^{-1}\left(\frac{B45}{2} \right) \right);$$

$$2.861439277 \tag{81}$$

Lastly, the physical lengths are calculated:

$$L1 := \frac{\psi 1}{\pi} \cdot \frac{\lambda g0}{2};$$

$$0.006220548565 \tag{82}$$

$$L2 := \frac{\psi 2}{\pi} \cdot \frac{\lambda g0}{2};$$

$$0.006651049750 \tag{83}$$

$$L3 := \frac{\psi 3}{\pi} \cdot \frac{\lambda g0}{2};$$

$$0.006678293470 \tag{84}$$

$$L4 := \frac{\psi 4}{\pi} \cdot \frac{\lambda g0}{2};$$

$$0.006651049750 \tag{85}$$

$$L5 := \frac{\psi 5}{\pi} \cdot \frac{\lambda g0}{2};$$

$$0.006220548565 \tag{86}$$